Cell Reports

Article

Methionine metabolism regulates pluripotent stem cell pluripotency and differentiation through zinc mobilization

Graphical abstract

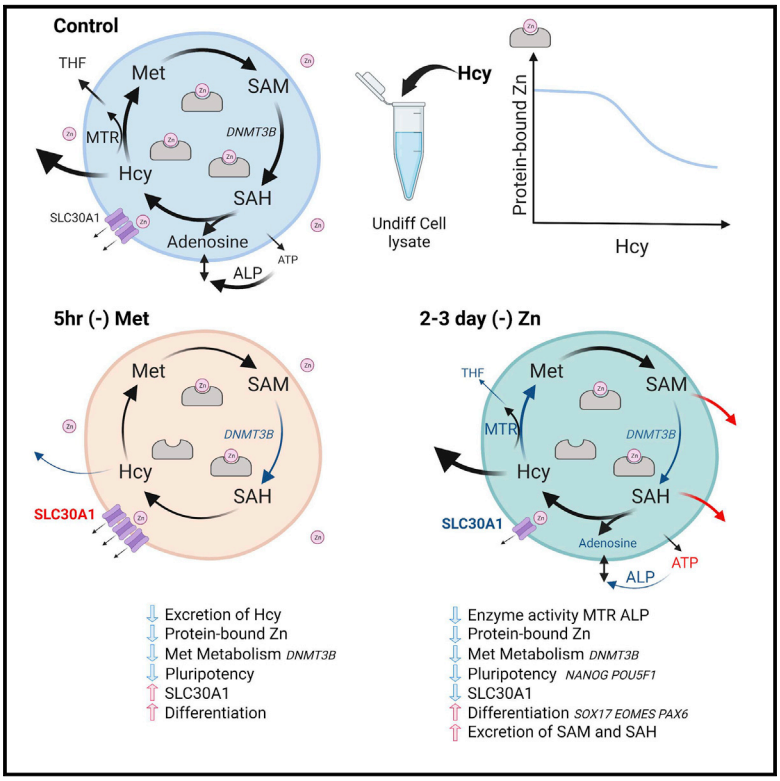

Highlights

- Methionine depletion of PSCs reduces protein-bound Zn through homocysteine
- Zn depletion of PSCs mimics methionine depletion and shows impaired pluripotency
- Zn depletion impairs proliferation and potentiates endoderm differentiation of PSCs
- PSCs cultured in Zn depletion showed altered methionine metabolism

Authors

Erinn Zixuan Sim, Takayuki Enomoto, Nobuaki Shiraki, ..., Mizuho Yokoyama, Masayuki Miura, Shoen Kume

Correspondence

shiraki@bio.titech.ac.jp (N.S.), skume@bio.titech.ac.jp (S.K.)

In brief

Pluripotent stem cells (PSCs) are highly dependent on methionine. Sim et al. show that Zn signaling lies downstream of methionine metabolism. Methionine depletion of PSCs triggers a decreased intracellular protein-bound Zn. Zn depletion of PSCs mimicked the effects of methionine depletion, leading to impaired pluripotency and proliferation.

Sim et al., 2022, Cell Reports *40*, 111120
July 19, 2022
https://doi.org/10.1016/j.celrep.2022.111120

CellPress

Cell Reports

CellPress
OPEN ACCESS

Article

Methionine metabolism regulates pluripotent stem cell pluripotency and differentiation through zinc mobilization

Erinn Zixuan Sim,[1,6] Takayuki Enomoto,[1,6] Nobuaki Shiraki,[1,6,*] Nao Furuta,[1] Soshiro Kashio,[2] Taiho Kambe,[3] Tomonori Tsuyama,[4] Akihiro Arakawa,[5] Hiroki Ozawa,[1] Mizuho Yokoyama,[5] Masayuki Miura,[2] and Shoen Kume[1,7,*]

[1]School of Life Science and Technology, Tokyo Institute of Technology, 4259-B-25 Nagatsuta-cho, Midori-ku, Yokohama, Kanagawa 226-8501, Japan

[2]Department of Genetics, Graduate School of Pharmaceutical Sciences, The University of Tokyo, 7-3-1 Hongo, Bunkyo-ku, Tokyo 113-0033, Japan

[3]Graduate School of Biostudies, Kyoto University, Kyoto 606-8502, Japan

[4]Division of Stem Cell Biology, Institute of Molecular Embryology and Genetics, Kumamoto University, Kumamoto, Japan

[5]Research Institute for Bioscience Products and Fine Chemicals, Ajinomoto, Kawasaki-shi, Kanagawa, Japan

[6]These authors contributed equally

[7]Lead contact

*Correspondence: shiraki@bio.titech.ac.jp (N.S.), skume@bio.titech.ac.jp (S.K.)

https://doi.org/10.1016/j.celrep.2022.111120

SUMMARY

Pluripotent stem cells (PSCs) exhibit a unique feature that requires *S*-adenosylmethionine (SAM) for the maintenance of their pluripotency. Methionine deprivation in the medium causes a reduction in intracellular SAM, thus rendering PSCs in a state potentiated for differentiation. In this study, we find that methionine deprivation triggers a reduction in intracellular protein-bound Zn content and upregulation of Zn exporter *SLC30A1* in PSCs. Culturing PSCs in Zn-deprived medium results in decreased intracellular protein-bound Zn content, reduced cell growth, and potentiated differentiation, which partially mimics methionine deprivation. PSCs cultured under Zn deprivation exhibit an altered methionine metabolism-related metabolite profile. We conclude that methionine deprivation potentiates differentiation partly by lowering cellular Zn content. We establish a protocol to generate functional pancreatic β cells by applying methionine and Zn deprivation. Our results reveal a link between Zn signaling and methionine metabolism in the regulation of cell fate in PSCs.

INTRODUCTION

Human embryonic stem cells (hESCs) and human induced pluripotent stem cells (hiPSCs) possess the ability for unlimited self-renewal and differentiation to yield cells derived from the three germ layers (Takahashi et al., 2007; Thomson et al., 1998). Upon adding specific growth factors, hESCs/iPSCs initiate differentiation and are converted into specific lineages. Recent progress in this field has successfully generated many functionally differentiated cell types and can be useful as alternative cell sources for cell replacement therapy, disease modeling, and drug discovery (Inoue et al., 2014; Sánchez Alvarado and Yamanaka, 2014; Takahashi and Yamanaka, 2016).

Type 1 diabetes results from the autoimmune destruction of insulin-producing pancreatic β cells, whereas type 2 diabetes results from progressive dysfunction and subsequent loss of these cells. Islet transplantation is an existing approach that provides better glycemic control (Gamble et al., 2018). However, this is hampered by the severe shortage of donor islets and lifelong immunosuppression requirements. Many research efforts have focused on identifying alternative sources that could replace β cells (Kieffer et al., 2017; Shapiro et al., 2017; Vieira et al., 2017; Zhu et al., 2016). Several stepwise differentiation protocols mimicking pancreatic differentiation have been established to differentiate hESCs or hiPSCs into pancreatic progenitor cells and insulin-expressing cells. These cells can produce and secrete insulin in response to high glucose (HG; Millman et al., 2016; Nair et al., 2019; Russ et al., 2015; Veres et al., 2019) and have been shown to reverse hyperglycemia when transplanted into diabetic mouse models (Pagliuca et al., 2014; Rezania et al., 2014; Velazco-Cruz et al., 2019). Although the hiPSC-derived pancreatic β cells have features resembling human endogenous pancreatic β cells, several characteristics still require improvements to generate more mature β cells. Marked variations have been reported in the differentiation capacities between hESC or iPSC cell lines (Nishizawa et al., 2016; Osafune et al., 2008). Elimination of such variations would therefore be beneficial. Here, we aimed to establish a protocol that would be applicable to different cell lines.

Stem cells possess a unique metabolic feature in which a change in their metabolic signatures modulates their epigenetic profile, leading to a change in gene expression and cell fate (Wu et al., 2016). While mouse ESCs exhibit unique threonine-dependent catabolism (Wang et al., 2009), threonine dehydrogenase is

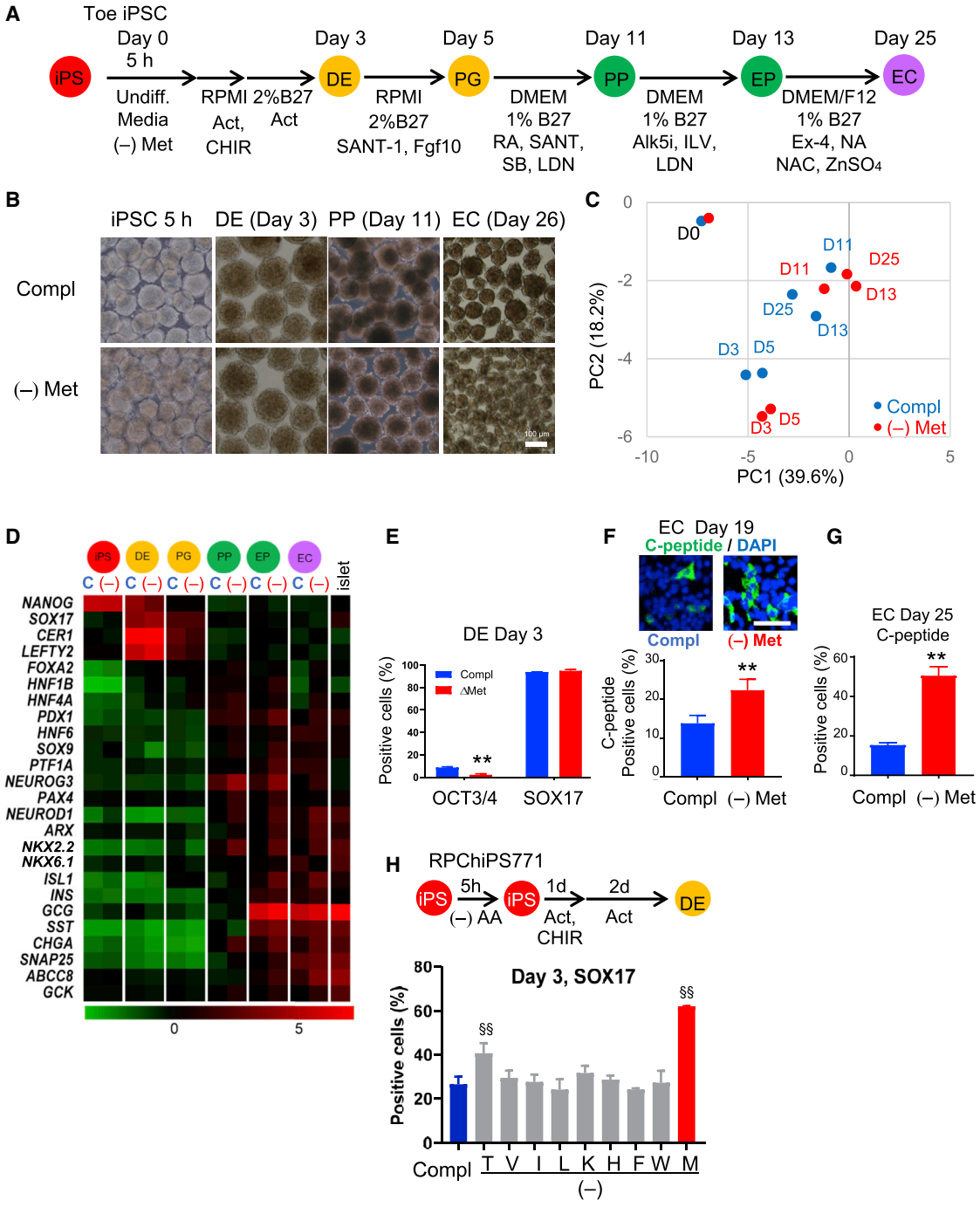

Figure 1. Methionine deprivation ((–) Met) pretreatment potentiated the differentiation of human iPSCs into insulin (INS)-expressing β cells

(A) Schematic drawing of the differentiation procedure using Toe hiPSCs.

(B) Representative bright-field images on days 0, 3, 11, and 26 of the differentiated hiPSCs. Scale bar: 100 μm.

(C) Gene array analysis data of the hiPSCs (D0), day 3 definitive endoderm (DE), day 5 primitive gut tube (PG), day 11 pancreatic progenitor (PP), day 13 endocrine progenitor (EP), and day 25 endocrine cell (EC) at (–) Met (red) or Compl (blue) condition (GEO: GSE 151794) were analyzed with principal-component analysis (PCA). Genes that contribute to PC1 and PC2 are shown in Table S1; contributions of PC1 and PC2: 39.6% and 18.2%, respectively.

(D) The maturation and differentiation-related gene expressions in the differentiated iPSCs, and human islets as a positive control, are shown by a heatmap. The top 10 Gene Ontology (GO) terms for the biological process of genes up- or downregulated by (–) Met compared to Compl are listed in Table S2.

(E) Immunocytochemical analyses of day 3 DE cells (dissociated and replated in monolayer for analysis) are presented as OCT3/4 or SOX17 positivity. N = 3.

(F and G) Representative C-peptide$^+$ stainings on day 19 (F) or day 25 (G) are shown. N = 3.

(legend continued on next page)

a pseudogene in humans. hiPSCs show a high requirement for methionine metabolism (Shiraki et al., 2014; Shyh-Chang et al., 2013). Methionine and threonine are metabolized to generate *S*-adenosylmethionine (SAM), which acts as a methyl residue donor and affects H3K4me3 levels. This process links the metabolic and epigenetic regulation of pluripotent hiPSCs (Shiraki et al., 2014; Shyh-Chang et al., 2013; Wang et al., 2009). A change in the metabolic state through methionine deprivation culture media renders pluripotent hiPSCs potentiated for differentiation, such that the cells show potentiated differentiation in response to inductive signaling (Shiraki et al., 2014).

We investigated the molecular mechanism underlying methionine deprivation-mediated potentiation of differentiation using microarray analysis and identified zinc (Zn) as a downstream target of methionine metabolism. Our study revealed that Zn plays a crucial role in controlling stem cell proliferation and differentiation. A decrease in intracellular protein-bound Zn content in iPSCs is a mechanism whereby methionine deprivation potentiates differentiation in undifferentiated cells. We propose a procedure to culture cells at a low Zn concentration to differentiate hiPSCs. The low Zn procedure is a powerful tool to eliminate undifferentiated hiPSCs and potentiate differentiation with methionine deprivation. Through gene expression profiling analysis and metabolite analysis, we revealed an interplay between methionine metabolism and Zn signaling in the cell fate regulation of hiPSCs.

RESULTS

Methionine deprivation ((–) Met) pretreatment potentiates late-stage differentiation of human iPSCs into insulin-expressing β cells

We previously reported that PSCs have a unique metabolic state that requires methionine metabolism. Deprivation of methionine in media rendered PSCs in a state biased toward differentiation, which readily shows increased differentiation upon signal induction. To explore whether (–) Met pretreatment could potentiate late-stage differentiation into pancreatic β cells, we differentiated Toe hiPSCs using a modified version of our previously reported procedure for generating insulin-expressing β cells (Nakashima et al., 2015; Shahjalal et al., 2014). After forming spheres, hiPSCs were treated for 5 h with the same medium (–) Met or control complete medium. Initiation of differentiation was induced by switching to differentiation media (Figure 1A). The differences in morphology of the differentiated cells between the (–) Met and control groups became apparent on day 26 endocrine cells (ECs). Large spheres appeared in control but not in the (–) Met-treated group, in which sphere sizes were more homogeneous (Figure 1B). Principal-component analysis (PCA) of time-dependent gene expression between (–) Met (red) and complete (blue) groups revealed increasing differences along PC1 in D13 and D25 (Figure 1C; Table S1). Analysis of individual gene expression in hiPSC-derived cells showed an increase in several pancreatic differentiation and maturation markers in D11 pancreatic progenitor (PP), D13 endocrine progenitor (EP), and D25 EC spheres pretreated with (–) Met compared to those of the controls (Figure 1D; Table S2). Immunocytochemistry analysis of the day 3 DE (D3DE [definitive endoderm]) cells revealed that (–) Met pretreatment significantly reduced the proportion of OCT3/4-expressing cells (Figure 1E). The increase in SOX17 positivity was not apparent, which may be due to the high differentiation efficiency into $SOX17^+$ cells of the hiPSC lines used. In (–) Met-pretreated cells, the proportion of ECs (day 19) staining positively for C-peptide, a by-product of *de novo* synthesized insulin (INS), significantly increased (Figure 1F), with approximately 50% of the day 25 ECs expressing C-peptide (Figure 1G). However, under this differentiation protocol, the expression of NKX6.1 was low. The optimization for the differentiation procedure was required.

Another hiPSC line, RPChiPS771, was used in which (–) Met and (–) Thr pretreatments were confirmed to significantly increase $SOX17^+$ cells in D3DE cells compared to other essential amino acid single deprivals (Figure 1H). Our results show that (–) Met pretreatment potentiates differentiation into endodermal and pancreatic fates.

Upregulation of *SLC30A1* expression as a downstream target of Met deprivation

To explore the upregulated genes upon (–) Met pretreatment, RNA was extracted from human 201B7 and Toe hiPSCs, cultured in complete or (–) Met medium for 5 h, and subjected to gene array profiling analysis. Compared with gene profiling results on KhES3 (Shiraki et al., 2014), we extracted 18 upregulated genes in all 3 cell lines (Figures 2A and 2B). FGF21 and SESN2 are reported to be upregulated by methionine or amino acid restriction (Ho et al., 2017; Luo et al., 2018), which concur with our results. *SLC30A1* was one of the genes upregulated in (–) Met-treated cells and encoded for the ZNT1 protein (Andrews et al., 2004), a Zn efflux transporter that localizes to the plasma membrane. Cellular Zn metabolism is regulated by uptake, efflux, and storage, which are regulated by its transporters encoded by two Zn transporter families, *Zrt- and Irt-like Proteins* (ZIP, *Solute Carrier 39A* [*SLC39A*]), Zn *Transporters* (ZNT, *SLC30A*), and Zn binding proteins, including metallothionein (MT). ZNT transporters promote Zn efflux from cells or into intracellular vesicles and reduce cytosolic Zn, whereas ZIP transporters promote the intake of Zn to increase cytosolic Zn.

We then reexamined our microarray analysis data (Figures 1C and 1D) of the *SLC30A1-10* and *SLC39A1-14* genes. Several members of the *SLC30A* or *SLC39A* are expressed in pluripotent iPSCs and differentiated hiPSC-derived pancreatic cells (Figure 2C). We then focused on the expression of *SLC30A* and *SLC39A* gene family members in hiPSCs. We examined whether their expression levels are affected in the short-term (5 h) deprival of Met or other single amino acid deprival using RPChiPS771 cells. *SLC30A1* was specifically upregulated >6-fold by (–)Met

(H) RPChiPS771 hiPSCs treated with (–) Met showed significantly increased SOX17 positivity, whereas other essential amino acids' single deprival, excluding Thr (T), did not. N = 3.

Data are expressed as means ± SDs. Two-tailed unpaired Student's t tests analyzed differences between groups, and significance is shown as $^{**}p < 0.01$ (E–G), or by 1-way ANOVA analysis followed by Dunnett's multiple comparisons tests; differences are shown as $^{§§}p < 0.01$.

A

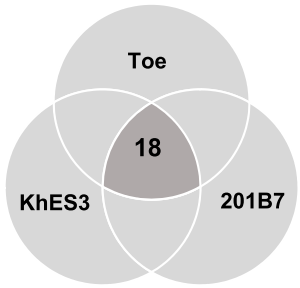

B

ALS2CR12	*Amyotrophic lateral sclerosis 2 chromosome region, candidate 12*
CBX4	*Chromobox homolog 4*
CEBPB	*CCAAT/enhancer binding protein (C/EBP), beta*
CHAC1	*ChaC, cation transport regulator homolog 1*
CSRNP1	*Cysteine-serine-rich nuclear protein 1*
CTGF	*Connective tissue growth factor*
DDIT4	*DNA-damage-inducible transcript 4*
DHRS2	*Dehydrogenase/reductase (SDR family) member 2*
EGR1	*Early growth response 1*
FGF21	*Fibroblast growth factor 21*
GADD45B	*Growth arrest and DNA-damage-inducible, beta*
RGS16	*Regulator of G-protein signaling 16*
SESN2	*Sestrin 2*
SLC30A1	***Solute carrier family 30 (zinc transporter), member 1***
STC2	*Stanniocalcin 2*
THBS1	*Thrombospondin 1*
TRIB3	*Tribbles pseudokinase 3*
ULBP1	*UL16 binding protein 1*

C

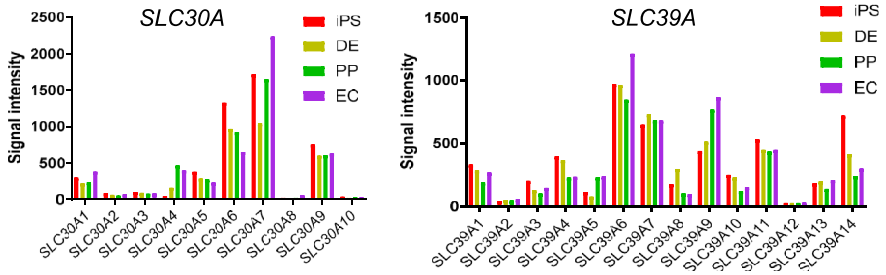

D

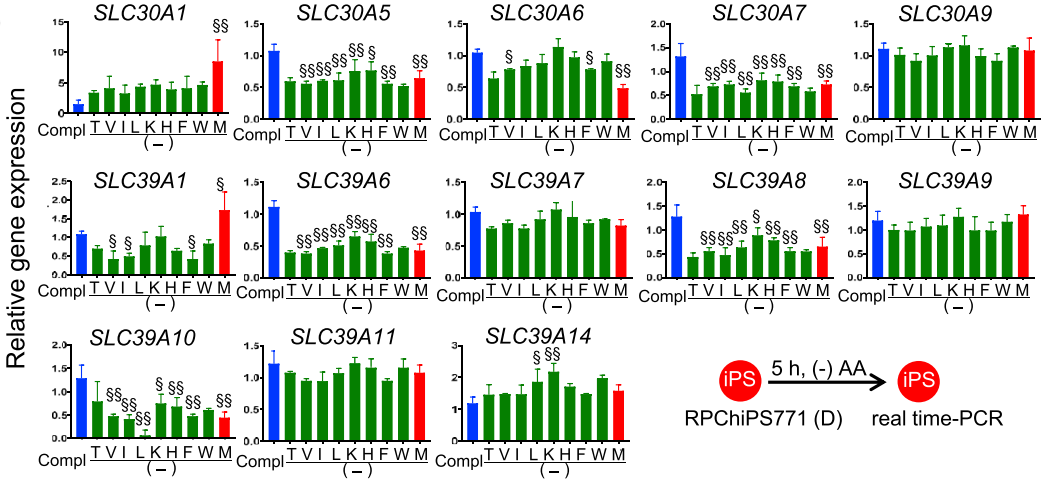

E

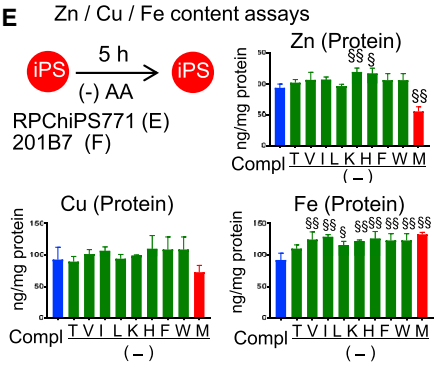

F

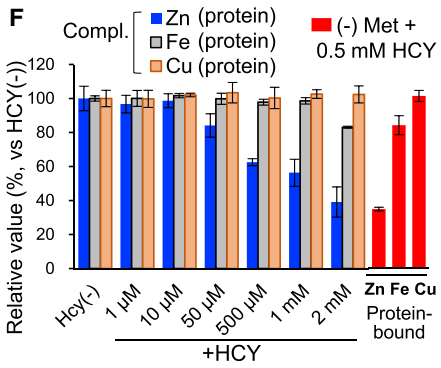

(legend on next page)

treatment (Figure 2D). *SLC39A1* was also upregulated, albeit to a smaller degree (>1.5-fold). Other *SLC30A* and *SLC39A* family members, including *SLC30A5*, *SLC30A6*, *SLC30A7*, *SLC39A6*, *SLC39A8*, and *SLC39A10,* showed decreased expression compared to the control, under the deprivation of both Met and other amino acids.

We then examined using a human ESC line the KhES3 and 201B7 hiPSC line and confirmed that 5 h (−) Met treatment triggered increased expression levels in the *SLC30A1* transcript (Figures S1A and S1B) and the ZNT1 protein (Figure S1C).

A reduction in intracellular protein-bound Zn was triggered by culturing pluripotent hiPSCs under Met or Zn deprival

ZNT1 localizes to the plasma membrane and excretes Zn. Increased ZnT1 may lead to a decreased intracellular Zn content. We then examined whether intracellular Zn content is affected by (−) Met. We measured the contents of intracellular heavy metals Zn, Cu, and Fe (labile or protein-bound forms) in pluripotent RPChiPS771 iPSCs treated with (−) Met or other single amino acids deprivals for 5 h (Figure 2E). As a result, a reduction in protein-bound Zn, but not labile Zn or other heavy metals, was observed under (−) Met conditions but not under the deprival of other single amino acids (Figure 2E).

Another iPSC line, 201B7, also used in our original gene array analysis, exhibited a reduced protein-bound Zn content and increased *SLC30A1* expression (Figures S2A and S2B) in response to (−)Met treatment. The decrease in protein-bound Zn content or upregulation of *SLC30A1* appears explicitly only in pluripotent iPSCs. In the human cervical epithelial carcinoma cell line HeLa, the human liver cancer cell line HepG2, or hiPSC-derived DE cells, (−) Met treatment did not lower protein-bound Zn content or upregulated *SLC30A1* expression (Figures S2C–S2H). However, these cancer cell lines and hiPSC-derived DE cells upregulated *EGR1* or *DHRS2* gene expression, which were identified as immediate-early responses to (−) Met conditions (Figures S2D, S2F, and S2H) (Shiraki et al., 2014).

Protein binding to Zn is mediated through the sulfur in the sulfhydryl group of cysteine (Kambe, 2019). Homocysteine (HCY) contains a sulfhydryl group and can replace Zn from its binding protein. We previously reported that under (−) Met conditions, hiPSCs ceased to excrete HCY (Shiraki et al., 2014). Under (−) Met conditions, a temporal increase in local HCY may occur that competed out Zn from its binding protein. Excess HCY added to the hiPSC lysate specifically reduced protein-bound Zn content but not protein-bound Fe or Cu in an *in vitro* experiment (Figure 2F). Using lysates from hiPSCs cultured under (−) Met, a lower HCY at 0.5 mM was enough to reduce the protein-bound Zn to a similar level at 2 mM HCY in iPSCs under Compl conditions. The result supports our hypothesis that the cessation of HCY excretion under (−) Met increased intracellular local HCY. The result suggests that Met metabolism regulates protein-bound Zn level through HCY.

Culturing pluripotent hiPSCs under Zn deprival triggered a reduction in pluripotency marker expression and increased differentiation marker expression

We previously reported that (−) Met triggers poised differentiation of PSCs (Shiraki et al., 2014). We hypothesized that the poised differentiation of PSCs is mediated through the reduced intracellular Zn content caused by (−) Met. We tested this possibility by reducing intracellular Zn concentration by culturing pluripotent hiPSCs in Zn-deprived ((−) Zn) media. We achieved (−) Zn by treating the medium with a chelating resin, Chelex 100, with a high affinity for polyvalent metal ions. We measured the content of the Zn, Co, Fe, Mg, and Ca, then replenished what was removed by Chelex 100 (Figure 3A). Pluripotent iPSCs were cultured in (−) Zn media for 24, 48, and 72 h, then, the cell number and Zn content were assayed. (−) Zn treatment of the iPSCs resulted in a minimum increase in cell number compared to the control after 72 h (Figure 3B, left). Intracellular protein-bound Zn content significantly decreased at 48 h and further reduced at 72 h (Figure 3B, right). These results suggest that the growth of pluripotent iPSCs requires Zn and that the intracellular Zn content can be manipulated by changing the Zn concentration in the medium. Real-time PCR analysis showed that the expression of genes essential for self-renewal or pluripotency of iPSCs, such as *LIN28A*, DNA methyltransferase 3B (*DNMT3B*), telomerase reverse transcriptase (*TERT*), and *ZFP42* (encoding a zinc finger protein, also known as *REX2*), are reduced in iPSCs cultured under (−) Zn conditions (Figure 3C). Conversely, the expression levels of genes associated with differentiation, such as eomesodermin (*EOMES*), SRY-box 17 (*SOX17*), cadherin 5 (*CDH5*), and LIM-homeodomain transcription factor Islet1 (*ISL1*), are upregulated under (−) Zn (Figure 3D).

iPSCs cultured under (−) Met conditions also showed reduced expressions of genes involved in self-renewal or pluripotency and increased expression of differentiation marker genes (Figure 3E). Our results, therefore, suggest that (−) Met triggers

Figure 2. (−) Met in pluripotent iPSCs triggered upregulation of *SLC30A1* and downregulation of protein-bound Zn contents

(A) Gene expression array analyses of pluripotent hiPSCs treated with (−) Met, or control complete medium with hiPSCs 201B7(GSE151795), Toe (GSE151794), are compared with the previous result with KhES3 ESCs (GSE55285) (Shiraki et al., 2014).

(B) Commonly upregulated genes in (−) Met groups.

(C) Expression profiles of *SLC30A and SLC39A* family genes in iPSCs or hiPSC-derived differentiated pancreatic cells revealed from our gene array analysis results.

(D) Real-time PCR analyses of the expression of *SLC30A and SLC39A* genes in pluripotent RPChiPS771 iPSCs upon deprivation of single amino acid. N = 3, excluding (−) Thr, (−) Trp (N = 2).

(E and F) RPChiPS771 (E) or 201B7 (F) were treated with (−) single amino acids (E) or (−) Met or (F) for 5 h and subjected to analysis of intracellular heavy metal contents of Zn, Cu, and Fe. Protein-bound Zn significantly decreased in iPSCs cultured under (−) Met but not in other (−) amino acid conditions. (F) Concentration-dependent HCY addition reduced protein-bound Zn (blue bars, Compl; red bars, (−) Met). (−) Met-treated iPSCs lysates required a lower HCY to reduce protein-bound Zn.

Data are expressed as means ± SDs. Differences are shown as $^{\S}p < 0.05$, $^{\S\S}p < 0.01$, analyzed by 1-way ANOVA Dunnett's multiple comparisons tests.

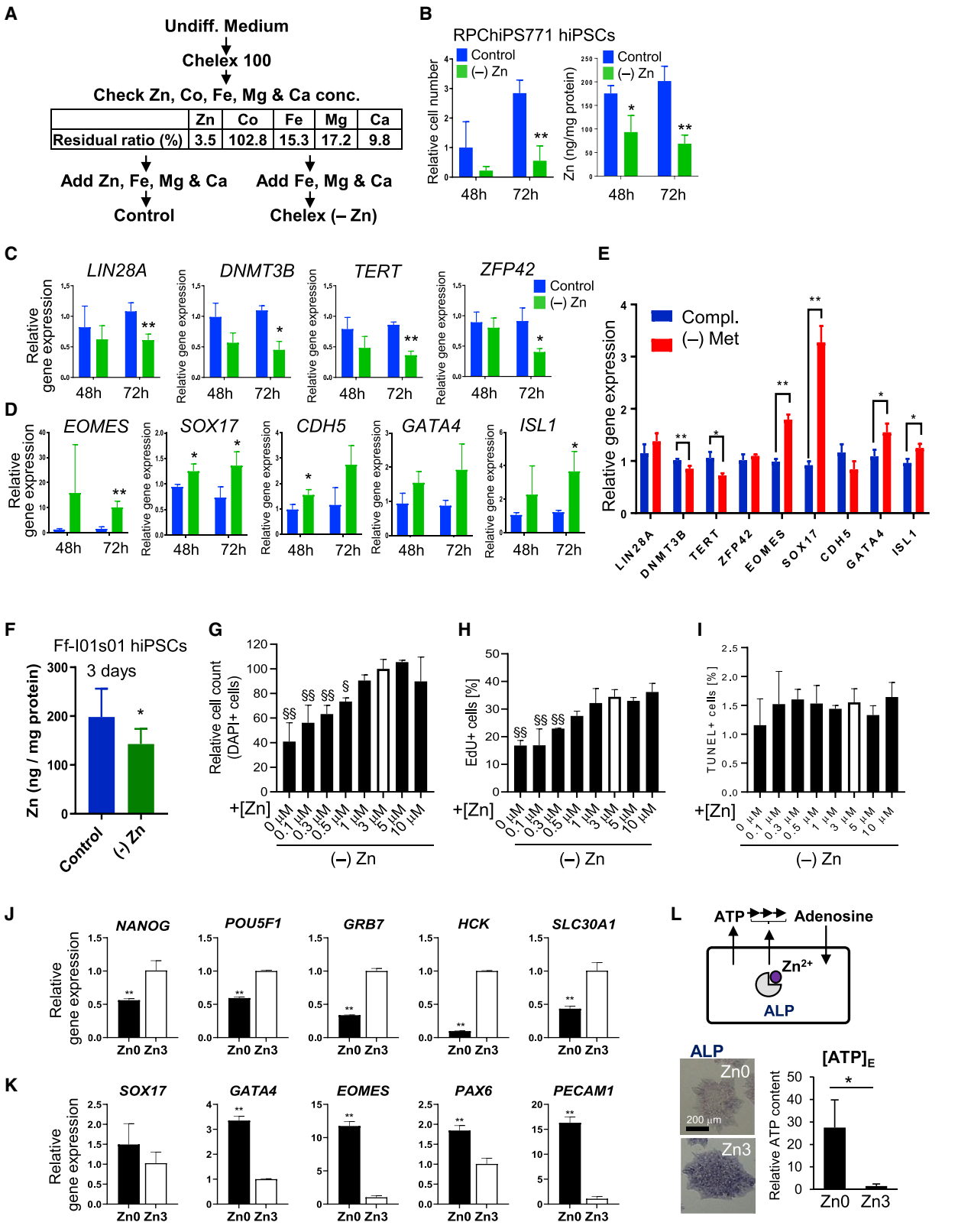

(legend on next page)

hiPSCs to exhibit a reduction in intracellular protein-bound Zn content. The similarity between gene expression patterns of iPSCs under (−) Zn and (−) Met conditions suggests that a decrease in protein-bound Zn is one of the downstream targets of the (−) Met condition.

We then developed a custom iPSC culture medium by which the Zn concentration could be controlled. Zn is used as a stabilizer for insulin (Brange et al., 1986), widely used as a supplement for sustaining cell growth and self-renewal of iPSCs. Our measurement revealed that the culture media of hiPSCs supplemented with insulin contains approximately 3 μM Zn. A custom-made (−) Zn basal medium (AKM (Zn0)) was tested to explore the use of insulin-like growth factor 1 (IGF1) to replace insulin. Ff-I01s01 hiPSCs cultured in the (−) Zn medium (AKM (Zn0)) for 3 days exhibited a decrease in protein-bound Zn (Figure 3F). We examined the effects on the growth and apoptosis of hiPSCs by comparing the supplementation of varying Zn concentrations in the medium (Figures 3G–3I). iPSCs showed a significant decrease in cell number upon culture under reduced Zn at 0.5 μM or lower (Figure 3G). 5-Ethynyl-2′-deoxyuridine (EdU) incorporation was significantly lower from below 0.3 μM Zn (Figure 3H), although no apoptosis occurred (Figure 3I).

After exposure to Zn deprival for 3 days (plated and cultured with (−) Zn medium), hiPSCs revealed the downregulation of pluripotency-related genes *NANOG* or *POU5F1*. Growth-related genes, growth factor receptor-bound protein 7 (*GRB7*), and hematopoietic cell kinase (*HCK*) were also downregulated at (−) Zn (Figure 3J). Reduction of *SLC30A1* in iPSCs cultured at (−) Zn was observed, suggesting that *SLC30A1* expression is tightly regulated by Zn (Figure 3J). Differentiation markers of the three germ layers were upregulated in hiPSCs at (−) Zn. The upregulated genes were endodermal markers *SOX17* and *GATA4*; a mesendoderm marker *EOMES*; an ectodermal marker *PAX6*; and platelet endothelial cell adhesion molecule (*PECAM1*; a mesoderm marker) (Figure 3K). These results suggest that iPSCs cultured at (−) Zn AKM (IGF1) conditions were in a state poised for differentiation, resembling that observed under (−) Met (Figure 3E).

We performed a knockdown experiment of *SLC30A1*. *SLC30A1* small interfering RNA (siRNA) transfected iPSCs showed reduced *SLC30A1* transcripts and ZNT1 protein but did not cancel the elevated expression of differentiation gene markers under (−) Met conditions (Figure S3). We confirmed that the increased expression of *MT1* genes responded to *SLC30A1* knockdown (data not shown), as previously reported in ZNT1-deficient cells, suggesting that intracellular Zn increased upon the reduction of ZNT1 (Nishito and Kambe, 2019). We interpret the result to mean that ZNT1 reduction is insufficient to inhibit the release of Zn from its binding protein under (−) Met conditions.

Zn deficiency was reported to impair the activities of the ectoenzymes, which led to a suppressed adenosine-nucleotide hydrolysis (Takeda et al., 2018). We then measured the activity of alkaline phosphatase (ALP), an ectoenzyme, and found that ALP activity decreased at Zn 0 μM compared to Zn 3 μM (Figure 3L, lower left). In coordination with the decreased ALP activity, extracellular ATP ($[ATP]_E$) increased significantly at Zn 0 μM (Figure 3L, lower right). The result demonstrates that Zn deficiency delayed extracellular ATP clearance and affects extracellular adenine nucleotide metabolism. The ALP activity is highly expressed in iPSCs and ESCs and is regarded as a unique and unambiguous biomarker of stem cells (Martins et al., 2014). The result demonstrates that (−) Zn impairs the pluripotency of hiPSCs and that ALP is one of the targets of Zn.

Zn deprival triggers potentiation of DE differentiation

To investigate the effects of (−) Zn on DE differentiation, we compared various Zn concentrations at 0, 0.5, or 3 μM, using AKM medium (M1-AKM (IGF1)) (Figures 4A and 4B). DE differentiation at Zn 0 μM resulted in low OCT3/4- and high $SOX17^+$ cells detected by immunocytochemistry. Zn concentrations at 0.5 or 3 μM led to increased OCT3/4 positivity and decreased SOX17 positivity. We also tested the effect of (−)Met in combination with (−) Zn. We found that a short 5-h (−) Met pretreatment before differentiation reduced OCT 3/4-expressing cells that appeared at Zn 0.5 or 3 μM culture conditions.

We examined the effects of (−) Zn on DE differentiation using eight hiPSC lines derived from HLA homozygote donors Ff-I01s01, Ff-I01s04, Ff-I14s03, Ff-I14s04, Ff-MH09s01, Ff-MH15s01, Ff-MH15s02, and Ff-MH23s01 (Sugita et al., 2016) (Figure 4C). When insulin (M1-AKM (INS)) was used, a substantial proportion of D3DE cells were OCT3/4 positive, although there was a cell line-to-cell line variation, as revealed by immunocytochemical analysis (Figure 4D). Upon culturing in (−) Zn during differentiation, $OCT3/4^+$ cells almost disappeared, revealing a high proportion of $SOX17^+$ cells (Figure 4E).

The combinatory effects of (−) Met and (−) Zn were confirmed using another hiPSC line, Ff-I14s04, and an hESC line, KhES3 (Figures S4A–S4C). We then examined the time-dependent appearance of $SOX17^+$ and $OCT3/4^+$ cells (Figures S4D and S4E). iPSCs showed an early increase in SOX17 positivity from day 1 at Zn 0 μM, compared to Zn 3 μM (Figure S4D). iPSCs

Figure 3. Culturing iPSCs under (−) Zn resulted in reduced proliferation, pluripotency, and increased differentiation marker expression that mimicked culturing iPSCs under (−) Met

(A–D) Preparation and culturing RPChiPS771 hiPSCs with (−) Zn medium by Chelex 100. (A) (−) Zn medium was prepared using Chelex 100. (B) Undifferentiated RPChiPS771 cells cultured with control or (−) Zn medium for 48 or 72 h were analyzed for relative cell number (left) or intracellular protein-bound Zn content (right). (C and D) Expression of gene markers for pluripotency and proliferation (C) or differentiation (D) in iPSCs treated with (−) Zn or control medium are shown.

(E) Expression of gene markers in cells treated with (−) Met for 5 h.

(F–L) Ff-I01s01 human iPSCs were cultured under a custom-developed medium AKM (IGF1). (F) Decreased protein-bound Zn content under culturing at (−) Zn was confirmed. (G) Cell number. (H) EdU incorporation. (I) Apoptosis (TUNEL assay). (J) Expressions of pluripotency and proliferation genes and *SLC30A1*. (K) Differentiation gene marker expressions. (L) Cells were analyzed for alkaline phosphatase staining (lower left) and extracellular ATP contents (lower right). Scale bar: 200 μm. (Zn0 refers to (−) Zn, Zn3 refers to (−) Zn with 3 μM Zn addition as controls.)

Data are expressed as means ± SDs, N = 3. Differences between groups were analyzed by 1-way ANOVA Dunnett's multiple comparison test; significances are shown as $^{\S}p < 0.05$, $^{\S\S}p < 0.01$ (G–I), or by 2-tailed unpaired Student's t test; differences are shown as $^*p < 0.05$ or $^{**}p < 0.01$, as compared between the (−) Zn or (−) Met and Compl control condition.

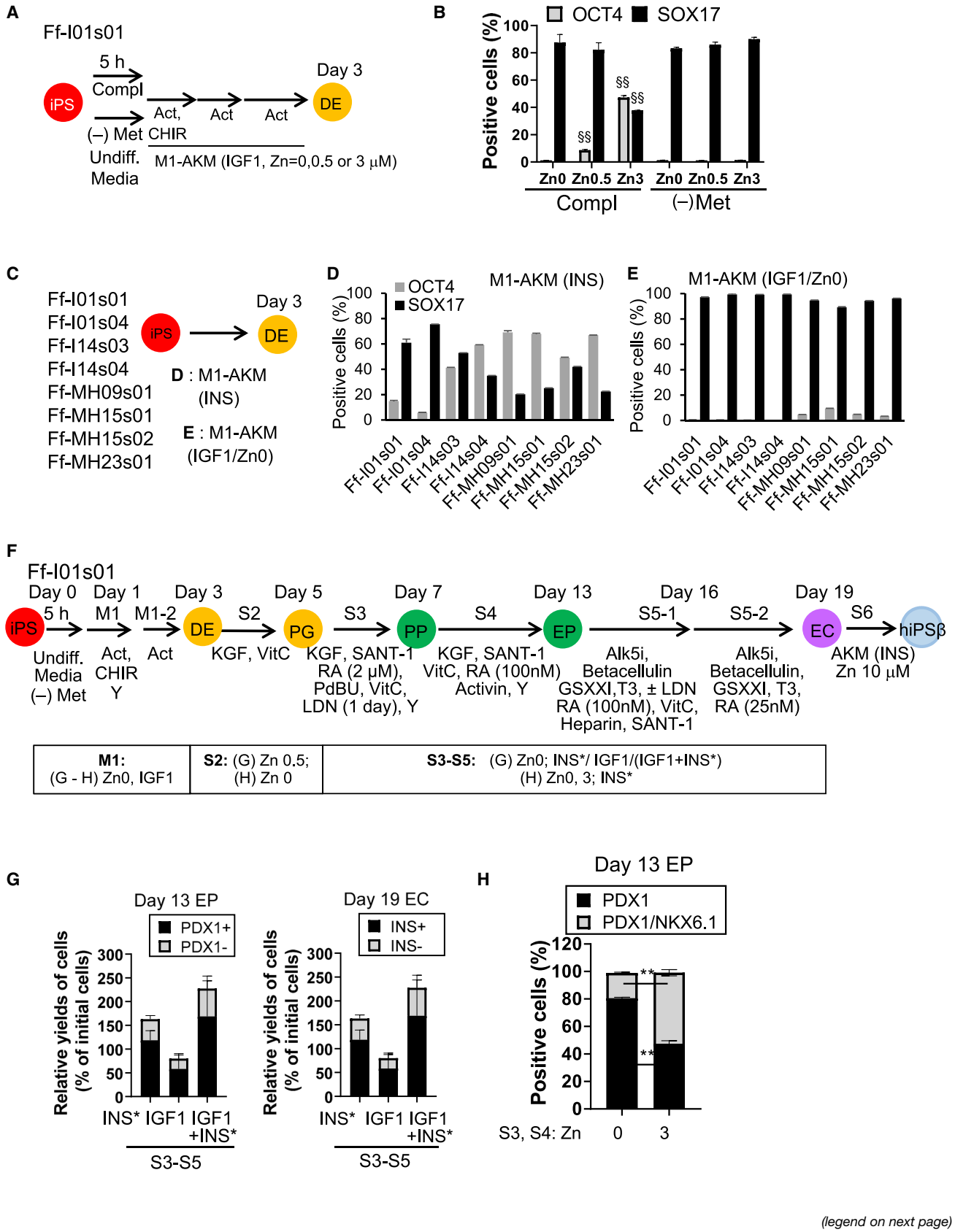

(legend on next page)

cultured at (−) Zn showed lower OCT3/4 positivity on days 2 and 3 than Zn 3 μM (Figure S4E). The results suggested that culturing hiPSCs at (−) Zn accelerated DE differentiation.

We then asked whether the (−) Zn condition potentiated differentiation into mesoderm and ectoderm besides endoderm differentiation. hiPSCs revealed an upregulated expression of mesoderm (*EOMES*) and ectoderm (*PAX6*) marker on day 0 under (−) Zn compared to the 3 μM Zn condition. However, after triggering to differentiate into mesoderm or ectoderm, their expression levels were not different between (−) Zn and 3 μM conditions (Figures S4F and S4G). The result indicates that the (−) Zn condition does not potentiate mesoderm or ectoderm but endoderm differentiation.

Optimization of Zn concentrations and growth factor supplements for pancreatic differentiation

To optimize the Zn concentration in subsequent pancreatic differentiation stages S3–S5, we used IGF1 or insulin glulisine (INS*), a rapid-acting insulin analog whose amino acid involved in Zn binding was mutated (Becker, 2007), as a growth factor supplement (Figures 4F–4H). Pancreatic differentiation was performed at Zn 0 μM for stage M1, 0 or 0.5 μM for stage S2, and then at Zn 0 or 3 μM for stages S3–S5 (Figures 4F–4H). We first examined the impact on cell numbers. Using the IGF1 supplement throughout stages S3–S5 gave lower EP cell numbers on day 13 (Figure 4G, left panel) and a lower EC number on day 19 than the INS* supplement (Figure 4G, right panel). The addition of INS* to the IGF1 condition rescued the low cell number of EP and EC cells (Figure 4G). Immunocytochemical analysis revealed that the proportion of pancreatic and duodenal homeobox 1^+ ($PDX1^+$) cells on day 13 or INS^+ cells on day 19 showed no differences between INS* or IGF1 conditions (Figure 4G). The results suggest that insulin supplementation is required for cell survival during the differentiation of primitive gut tube (PG) into EC cells. We then compared the effects of Zn concentrations at 0 or 3 μM during stages S3–S4 on pancreatic differentiation (Figure 4H) (stage S2, Zn 0 μM). The results revealed that cells cultured at Zn 3 μM (INS* supplemented condition) during stages S3–S4 tend to give rise to comparably higher $NKX6.1^+$ cells among $PDX1^+$ cells on day 13 (EP stage) (Figure 4H).

Our results suggest that IGF1 is permissive for differentiation but may not sufficiently support cell growth, particularly during the late stages S3–S5. Since using the INS, supplement yields a final concentration approximately equivalent to Zn 3 μM, we adopted the following conditions: IGF1/Zn 0 μM for endoderm differentiation (stage M1) and INS/Zn 3 μM for pancreatic differentiation (stages S3–S5).

We then compared the effects of the four conditions on pancreatic differentiation. In agreement with our above results, the presence of Zn during stage 1 (DE differentiation) significantly reduced $PDX1^+/NKX6.1^+$ EP cells, and combinatory treatment of (−) Met and (−) Zn significantly increased $PDX1^+/NKX6.1^+$ EP cells (Figure S4H). The results further support our finding that (−) Zn potentiates differentiation, which further acts in combination with (−) Met to enhance differentiation.

The generation of functional endocrine β cells under the (−) Zn and (−) Met protocol

We then adopted the protocol shown in Figure 4F, with M1 at Zn 0 μM (IGF1) and S3–S5 at Zn 3 μM (INS). Immunocytochemical analysis of stage-specific gene marker expression confirmed efficient differentiation to yield DE (day 3), pancreatic progenitor (PP) (day 8), EP (day 13), and EC (day 21) (Figure 5A). The proportions of cells expressing the differentiation markers are indicated in the figure (Figure 5A). We obtained over 99% of SOX17-expressing DE cells on day 3, 93% of PDX1-expressing PP cells on day 8, 48.8% ± 2.3% NKX6.1-expressing EP cells on day 13, and 79.6% ± 0.76% INS-expressing EC cells on day 21. The hiPSβ spheres on day 36 showed an islet-like structure (Figure 5B). Gene expression analysis by real-time PCR revealed differentiation marker expression in a stage-dependent manner in the differentiated cells and hiPSβ. Gene expressions are presented as fold changes compared to human islets (human islet = 1), with the heatmap showing the expression range of the genes (Figure 5C). High levels of *NANOG* expression in undifferentiated iPSCs, *SOX17* in DE stage, *SOX9*, and *PDX1* in PP and EP stages. *NGN3* expression peaks at the EP stage and sustained in the EC stage, followed by *CHGA* and *INS* expression from EC stage (day 21) and further upregulation in hiPSβ (day 36) were observed, with *INS* expression in hiPSβ at a level comparable to that in human islets (Figure 5C). Stage-dependent expression profiles of the markers during stages S3–S6 (iPSβ) demonstrate that the hiPSβ cells exhibit a characteristic expression profile like that of human islets (Figure S5).

After reaggregation (at the end of stage S5), 34.8% ± 1.62% $INS^+/NKX6.1^+$ (double-positive) cells existed in hiPSβ at day 36. There are certain populations of INS^+/GCG^+ (43.2% ± 0.77%) and INS^+/SST^+ (somatostatin positive; 17.2% ± 1.9%) in the hiPSβ (Figure 5D). We compared the expression in several cohorts of hiPSβ cells (days 26–39), without (cohort 1) or with (cohorts 2 and 3) dissociation and reaggregation at the end of stage S5 (Figure 5E). hiPSβ cells expressed *INS*, *PDX1*, *NKX6.1*, and *UCN3* at levels similar to those in human islets. The expression level of *GCG* was higher than and *MAFA* was

Figure 4. Optimization of Zn concentration and IGF1 or INS supplements for differentiation into endoderm and pancreatic endocrine cells

(A and B) Schematic drawing of DE differentiation (A). Ff-I01s01 human iPSCs were differentiated into DE by culturing under M1-AKM (IGF1/Zn0, 0.5, or 3 μM), with or without (−) Met pretreatment (B).

(C–E) Schematic drawing of culture conditions (C). Differentiation into DE under M1-AKM (INS) (D) or M1-AKM (IGF1/Zn0) (E). OCT3/4 or SOX17 positivities are shown.

(F) Schematic drawing of the culture procedure to obtain INS^+ EC cells from Ff-I01s01 hiPSCs.

(G and H) Zn concentrations, IGF1, or INS* supplement used in the basal medium are shown at the bottom of the panels. (G) Total cell numbers were compared among INS*, IGF1, or IGF1+INS* supplemented conditions during S3–S5 and assayed on day 13 (left panel) or day 19 (right panel). (H) Zn concentrations at 0 and 3 μM during S3–S4 were compared, and the ratio of $PDX1^+$ cells (left panel) or $PDX1^+NKX6.1^+$ double-positive cells (right panel) are shown.

Data are expressed as means ± SDs. N = 3. Differences between groups were analyzed by (B) 1-way ANOVA Dunnett's multiple comparisons tests; significances are shown as $^{§§}p < 0.01$ or (H) 2-tailed unpaired Student's t test; differences are shown as $^{**}p < 0.01$.

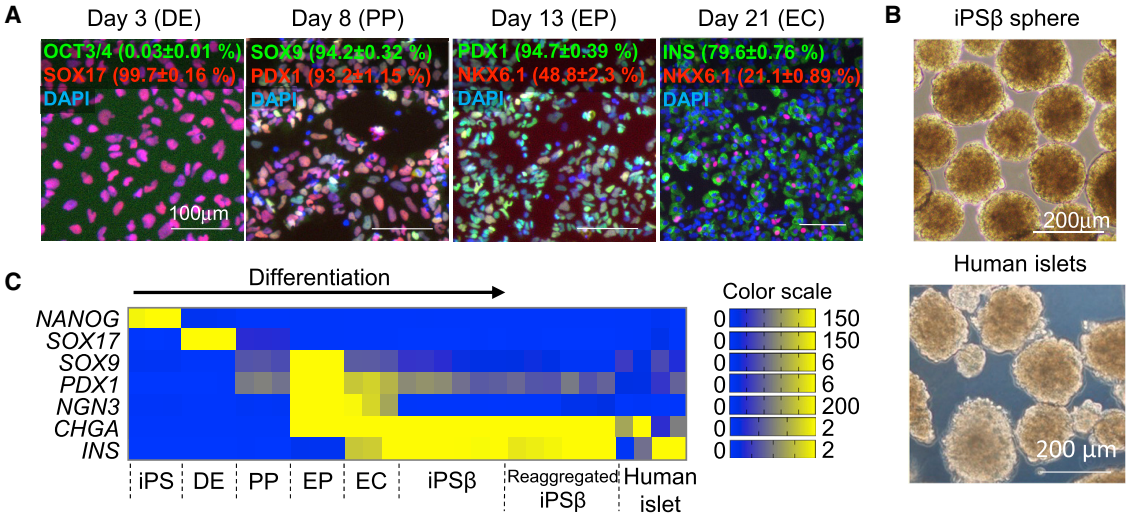

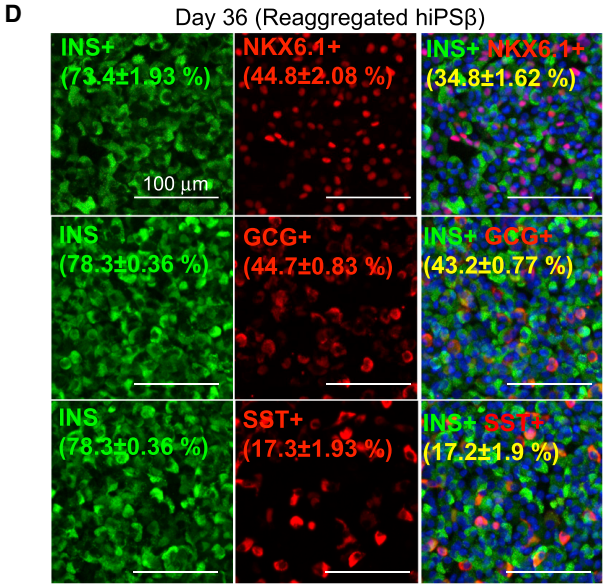

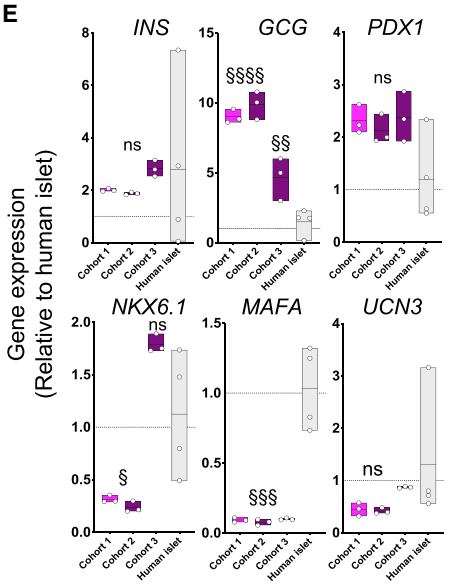

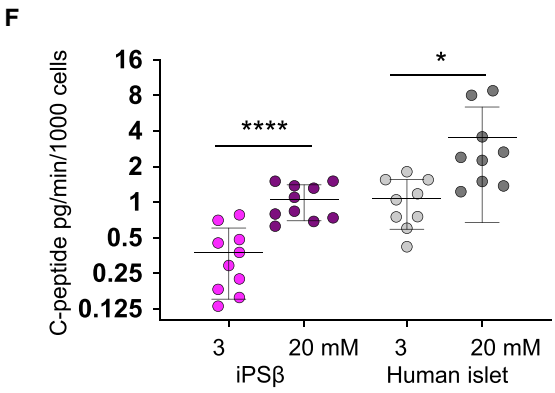

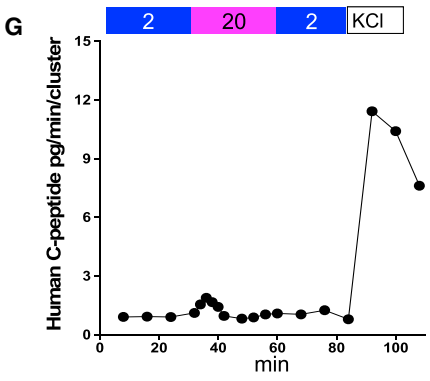

(legend on next page)

lower than that of human islets (Figure 5E). A glucose-stimulatory insulin secretion (GSIS) assay was performed with the reaggregated hiPSβ to test the functionality. The results revealed that the resultant hiPSβ (day 35) responded to HG and showed GSIS approximately 3.5-fold lower than that of the human islets (Figure 5F). The stimulation index in hiPSβ (ratio of GSIS at HG versus low glucose [LG]) is 2.77, which is slightly lower than that of the human islets at 3.29. A dynamic GSIS examination of the time-dependent response to glucose stimulation of hiPSβ revealed a quick first-phase insulin secretion in response to HG concentration. In addition, it showed a response to KCl stimulation (Figures 5G and S6A). Our results, therefore, revealed that our (−) Met and (−) Zn procedure is applicable for the generation of pancreatic endocrine β-like cells capable of GSIS activity.

We performed pancreatic differentiation following a protocol reported by other groups (Velazco-Cruz et al., 2019), using an MCDB131 medium that contained a low concentration of Zn (approximately 0.001 μM) and supplied with a low ITS-X (1:50,000). Under this protocol, the yielded hiPSβ cells show a gene expression profile (Figure S6B), morphology, and GSIS activity similar to our protocol (Figures S6C and S6D). Our results that (−) Zn condition potentiates differentiation into endoderm and pancreatic cells provide the rationale that using MCDB131 could successfully derivate endocrine β cells from hiPSCs.

A link between Zn signals and methionine metabolism

To understand the impact of Zn on gene expression, we performed RNA sequencing (RNA-seq) to analyze the global expression profile of pluripotent hiPSCs after culturing for 2 days under graded concentrations of Zn (0, 0.5, 3, and 10 μM) (Figures 6A and S7A). A total of 1,136 genes were upregulated (>1.3-fold) and 1,653 genes were downregulated (<0.77-fold) significantly ($p < 0.05$) at 10 μM Zn compared to 0 μM Zn. Gene Ontology (GO) enrichment analysis of the upregulated or downregulated genes was performed. The top 10 gene categories are shown in Figures 6B and 6C, with the full gene names listed in Tables S3 and S4, respectively. The Zn-dependent upregulated gene categories include cellular Zn ion homeostasis, mitochondrial translational elongation, and termination. The upregulated genes contain MT family members, such as *MT1X*, *MT1H*, *ATP7B*, *MT2A*, *MT1G*, *MT1E*, and *SLC30A1*genes. The upregulated genes also include mitochondrial ribosomal proteins *MRPL39*, *MRPL 23*, *GADD45GIP1*, and *MRPL24*, among others (Figure 6B; for full gene names and accession nos., see Table S3). The MT family genes and *SLC30A1* are targets of the Zn-dependent transcription factor MTF-1, which heads a hierarchy of gene responses to Zn (Choi and Bird, 2014; Hardyman et al., 2016'; Gonzalez-Iglesias et al., 2014), while the ribosomal proteins are known to comprise a Zn-binding domain and serve as the main Zn store (Hensley et al., 2011, 2012). The expression of the representative genes in response to Zn is presented in bar graphs in Figure S7B.

Gene categories of the genes downregulated by Zn include the regulation of autophagy, actin filament, synapse assembly, and cellular response to starvation (Figure 6C; Table S4). Representative gene expressions in response to Zn are shown in Figure S7C. These results suggest that cells possess a regulatory circuit to maintain Zn homeostasis through transcriptional and translational controls to regulate cell growth and cellular response. We also observed changes in the expression of genes related to signal transductions under (−) Met condition (H.O. and N.S., unpublished results).

Zn-responsive genes in the pluripotent hiPSCs (the present study) were examined and compared with the genes affected by (−) Met in hESCs (Shiraki et al., 2014). We compared the 594 genes upregulated by >1.5-fold under (−) Met with the Zn-responsive genes. Genes upregulated by (−) Met showing a high correlation with increasing Zn are listed in Table S5 (coefficient of determination $|R^2| > 0.70$). Several genes were positively correlated in response to increasing Zn concentrations, including *EGR1*, *MT1H*, *PIM1*, *SLC30A1*, and *TNFRSF12A* (Figure 6D; Table S5). Among the five MT family genes upregulated by Zn in hiPSCs, *MT1H* is a (−)Met upregulated gene. In contrast, of the 733 genes downregulated by <0.67-fold under the (−) Met condition in hESCs/hiPSCs, genes showing a high correlation with Zn are listed in Table S6 (coefficient of determination $|R^2| > 0.70$). Thirty-eight genes were negatively correlated in response to Zn (Figure 6E). Commonly downregulated genes were *FLT1*, *GDF3*, *P2RY1*, *SLC39A6*, *TET1*, and *USP12* (Figure 6E; Table S6).

We also examined genes related to the methionine and cysteine cycle. Methionine adenosyltransferase 2A (*MAT2A*) is upregulated, whereas *DNMT3B* is downregulated by Zn deprival (Figure 6F). We previously reported (Shiraki et al., 2014) the upregulation of *MAT2A* and downregulation of *DNMT3B* under (−) Met (Figure 6G). The effects of Zn and Met deprivals on the changes in *MAT2A* and *DNMT3B* expressions seem to be

Figure 5. The use of Zn and (−) Met medium to generate functional endocrine β cells

(A) Immunocytochemical analysis of marker expression. Representative images are shown. OCT3/4 (green), SOX17 (red), SOX9 (green), PDX1 (red or green), NKX6.1 (red), INS (green), and nuclei (DAPI, blue). N = 3 (biological replicates). Scale bar: 100 μm.

(B) A representative image of the hiPSβ spheres (upper) and the human islets (lower). Scale bar: 200 μm.

(C) A heatmap presentation of marker expressions shown as fold changes compared to human islets. The color scales on the right show the expression range of the genes on the left. N = 3 or 6 for iPSβ (biological replicates).

(D) Immunocytochemical analysis of endocrine marker expression in hiPSβ (day 36). Numbers indicate the percentage of positivity of stainings. N = 3 (biological replicates). Scale bar: 100 μm.

(E) The expression levels of the indicated genes at stage 6 hiPSβ (days 36–39, purple boxes) compared to human islets (gray boxes). Cohort 1 (−), cohorts 2 and 3 (+) dissociation and reaggregation at the end of stage 5. Individual data (N = 3, biological replicates) are plotted as fold changes compared to human islets, shown as floating bar plots. One-way ANOVA test, Dunnett's multiple comparisons test (versus human islet). Significant differences between groups are shown as $^{§}p < 0.05$, $^{§§}p < 0.01$, $^{§§§}p < 0.001$, $^{§§§§}p < 0.0001$. ns, not significant.

(F and G) Static GSIS activities on day 35 (F) or dynamic GSIS on day 38 (G) of the reaggregated hiPSβ. (F) Low glucose (LG, 3.0 mM; pink, light gray) and high glucose (HG, 20 mM; purple, dark gray) of the hiPSβ and human islets were compared. A 2-tailed paired t test analyzed differences between groups, shown as $^{*}p < 0.05$, $^{****}p < 0.0001$. (G) Time-dependent responses to LG (2.0 mM; blue) or HG (20 mM; pink) or KCl (white) are shown. Individual data are plotted.

A

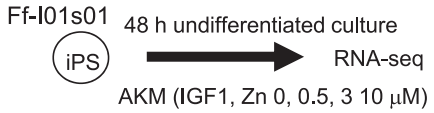

B

Category	P-value
cellular zinc ion homeostasis	2.73E-08
mitochondrial translational elongation	1.70E-07
mitochondrial translational termination	1.85E-07
detoxification of copper ion	3.19E-07
mitochondrial large ribosomal subunit	8.59E-07
negative regulation of growth	8.98E-07
cellular response to zinc ion	2.10E-06
embryonic digestive tract development	3.05E-06
cellular response to copper ion	8.02E-06
cellular response to cadmium ion	3.50E-05

C

Category	P-value
regulation of autophagy	5.98E-11
actin filament	3.86E-09
synapse assembly	1.20E-08
cellular response to starvation	3.45E-08
regulation of neuron projection development	2.48E-07
circadian rhythm	3.12E-07
protein processing	5.68E-07
atpase-coupled intramembrane lipid transporter activity	1.09E-06
response to endoplasmic reticulum stress	1.80E-06
cellular response to drug	2.03E-06

D Genes upregulated by (–) Met and cytosolic Zn

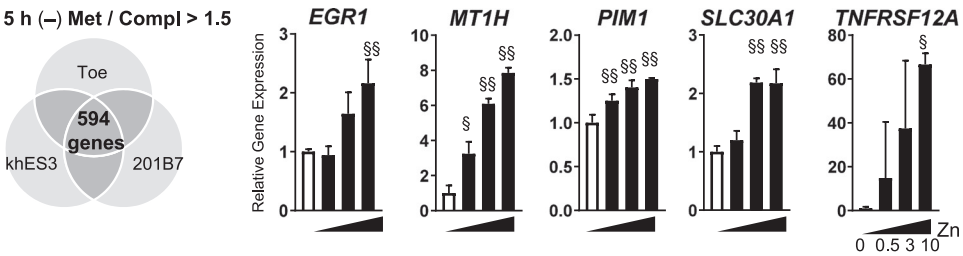

E Genes downregulated by (–) Met and cytosolic Zn

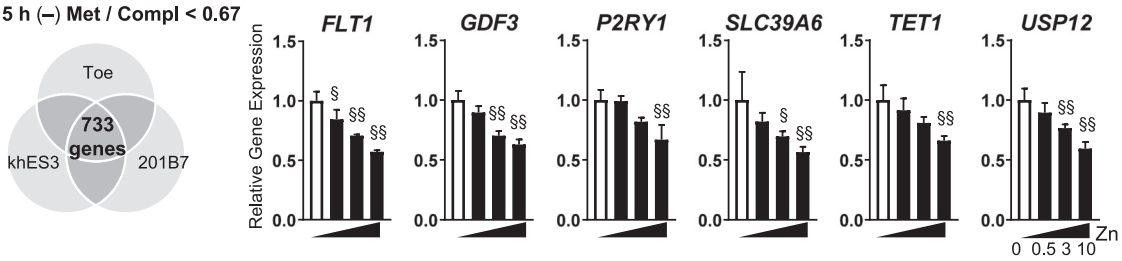

F

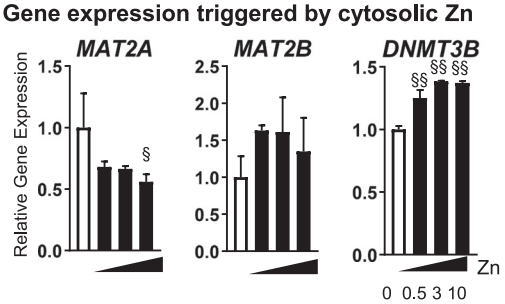

G

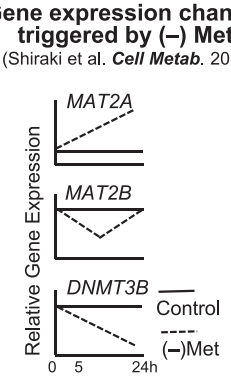

H

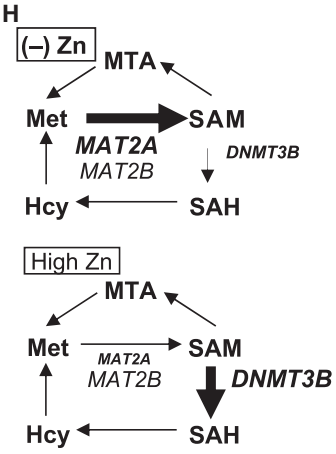

(legend on next page)

parallel. Our results reveal that pluripotent iPSCs sense environmental Zn changes in a manner resembling their response to methionine changes and rapidly elicit transcriptional changes. *MAT2A* and *DNMT3B* expressions could be markers that iPSC is sensing extracellular Zn levels.

An interdependent relationship between Met metabolism and Zn signaling

We then examined the changes in the methionine metabolism-related metabolites that existed intracellularly and in the medium, between (−) Zn and 3 μM Zn. There was a significant decrease in intracellular adenosine ($[Adenosine]_i$) at (−) Zn compared to 3 μM Zn (Figure 7A). Adenine-nucleotide hydrolysis is mediated by a Zn-dependent ALP, whose activity is downregulated upon Zn deprival (Figure 3L). Therefore, the decreased $[Adenosine]_i$ reflects the decreased adenine-nucleotide metabolism under Zn deficiency. By contrast, in the medium, many amino acids and metabolites significantly differed between iPSCs cultured in (−) Zn and 3 μM Zn (Figure 7B). Since the medium contains methionine and other amino acids that cells consume accompany cell growth, we subtracted from our measurements the initial amounts of the metabolites existing in the fresh medium and normalized the values to 24 h and the cell number. A minus value represents the consumption by the cells, and a plus value represents the excretion from the cells (nmol/24 h/1 × 10^6 cells). The metabolites and amino acids changed were as follows: Methyl-thio-adenosine ($[MTA]_E$), $[SAM]_E$, *S*-adenosyl-homocysteine ($[SAH]_E$), $[Glycine]_E$, and tetrahydrofolate ($[THF]_E$).

Betaine homocysteine *S*-methyltransferase (BHMT) and 5-methyl-tetrahydrofolate-homocysteine methyltransferase (MTR) are Zn-dependent enzymes. BHMT and MTR catalyze the conversion of HCY to methionine and require Zn for their catalytic activities (Evans et al., 2002; González et al., 2004; Koutmos et al., 2008). The reduction of $[THF]_E$ at (−) Zn indicated the inhibition of MTR and that HCY conversion to methionine is inhibited. The reduction of $[Adenosine]_i$ at (−) Zn indicated the inhibition of SAH conversion to HCY. The HCY excretion was not inhibited at (−) Zn, denoting that an accumulation at HCY occurred. iPSCs uptake methionine supplied in the medium and metabolize to SAM, and SAH, thereby maintaining the intracellular contents of these metabolites. The results suggest that accumulation of HCY occurred under (−) Zn, which triggered a "traffic jam" (a decreased flow) of the methionine metabolism. HCY is a toxic metabolite; cells sense HCY accumulation and excrete the HCY. The excreted HCY is ∼1/8-fold of the methionine consumed and ∼4-fold of SAM excreted from the cells. Taken together, our results suggest that Zn and Met metabolisms are interdependent.

DISCUSSION

Integration of methionine metabolism and Zn signaling

Zn is an essential cofactor in many enzymes. Potentially, 10% of the human proteome is Zn binding (Andreini et al., 2006). Many transcription factors contain structural domains that Zn stabilizes (Choi and Bird, 2014; Fukada et al., 2011; Kambe et al., 2014, 2017; Kimura and Kambe, 2016; Yamasaki et al., 2007). Zn binds to many proteins and acts in a regulatory or catalytic manner (Anzellotti and Farrell, 2008; Krężel and Maret, 2017). MTR and BHMT are Zn-dependent enzymes that possess a catalytic Zn center essential for activating the thiolate species of the HCY substrate, then bind and transfer the methyl residue to HCY to form methionine (Abdel-Azeim et al., 2011; Koutmos et al., 2008). MTR catalyzes methyl transfer from *N*-methyl-tetrahydrofolate (5M-THF) to HCY (Koutmos et al., 2008). BHMT catalyzes methyl transfer from betaine to HCY (Evans et al., 2002). Intracellular HCY was under detection. We detected extracellular HCY ($[HCY]_E$) at a certain level even in (−) Zn conditions. iPSCs excreted HCY, SAM, and SAH, which were not observed under the 3-μM Zn condition. The result suggested that iPSCs cultured in (−) Zn conditions exhibited an altered methionine metabolism.

From our RNA-seq results, MT family members and several members of the *MRPL* gene family are the top genes that are upregulated by increasing Zn concentrations in hiPSCs. MTs are known to bind 7 Zn atoms, participate in the control of cellular Zn metabolism, store Zn, and donate Zn to its target apo-metalloproteins (especially Zn finger proteins and enzymes). Adequate expression of these MTs may be essential to maintain Zn at a proper range for cell growth and function maintenance. Ribosomal proteins are reported to function as Zn storage, are involved in Zn homeostasis, and act as Zn sensors in translational regulation (Danchin, 2020; Hensley et al., 2012).

We found that (−) Met upregulated the transcription level of the exporter *SLC30A1* (Figure 2). Increasing Zn also upregulates *SLC30A1* expression (Table S5). These results suggest that (−) Met treatment of hiPSCs may trigger a transient increase in cytosolic Zn, possibly by reducing protein-bound Zn, which upregulates the exporter *SLC30A1* expression. *N*-Glycosylation post-transcriptionally controls ZNT1 protein expression on the cell surface in response to cellular Zn levels (Nishito and Kambe, 2019). Therefore, ZNT1 is regulated transcriptionally and post-transcriptionally to ensure tight control of intracellular Zn levels.

Many genes are commonly downregulated at high Zn concentrations and (−) Met conditions. Zn importer *SLC39A6* is one of the genes downregulated by (−) Met and high Zn, suggesting that transient high Zn might occur by (−) Met treatment, likely

Figure 6. A link between Zn signal and methionine metabolism

(A) Schematic drawing of the iPSC culture conditions for RNA-seq.

(B and C) The top 10 categories from GO enrichment analysis for upregulated (B) or downregulated (C) genes by increasing Zn.

(D and E) The representative gene expression profiles upregulated (D) or downregulated (E) by (−)Met and increasing Zn. (D) Of the 594 genes commonly upregulated >1.5-fold by (−) Met in at least 2 different array sets, representative genes showed a high correlation with increasing Zn are shown. (E) Of the 733 genes commonly downregulated <0.67-fold by (−) Met in at least 2 different array sets, representative genes negatively correlated to Zn are shown.

(F–H) Decreased expression of *MAT2A* and increased expression of *DNMT3B* were observed with increasing Zn concentrations (F). (−) Met upregulates *MAT2A* and downregulates *DNMT3B* (G). Under (−) Zn or (−) Met, iPSCs upregulate *MAT2A* expression to increase SAM. In contrast, under high Zn- or Met-fed conditions, iPSCs upregulate *DNMT3B* to consume SAM (H).

Data are expressed as means ± SDs. N = 3 (biological replicates). Differences between groups were analyzed by 1-way ANOVA Dunnett's multiple comparison tests, and significant differences are shown as $^{\S}p < 0.05$, $^{\S\S}p < 0.01$.

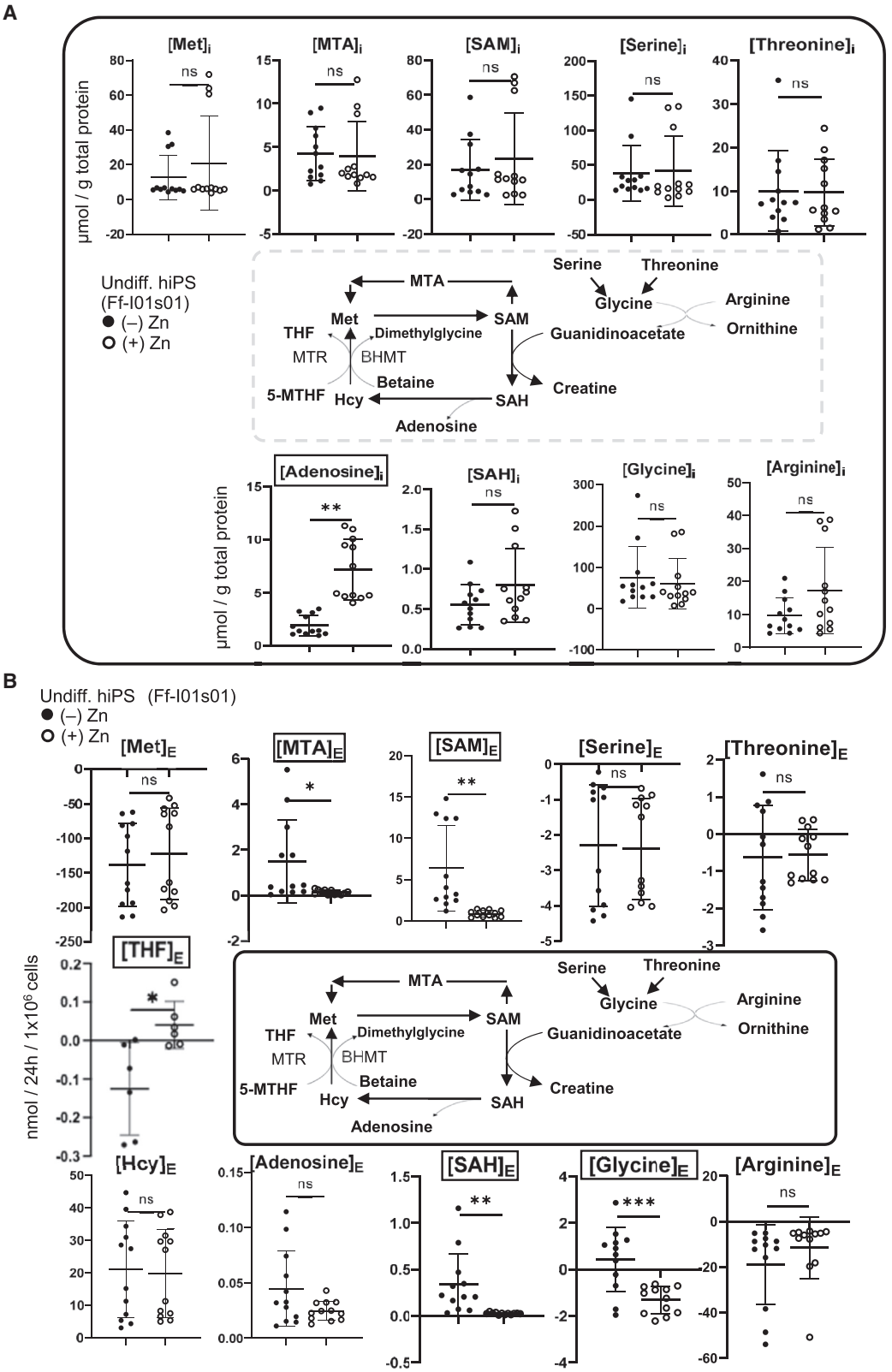

(legend on next page)

through displacing Zn with HCY from Zn-binding protein. Cytosolic labile Zn increased under the (−) Met condition, which upregulated MT expressions. The effect of (−) Met on potentiating endoderm differentiation was not canceled by Zn 3 μM, suggesting that increasing cytosolic labile Zn cannot rescue the reduced protein-bound Zn contents under (−) Met condition. This result agrees with our *SLC30A1* knockdown experiments.

Our finding that the gene expression of methionine-cysteine cycle enzymes *MAT2A* and *DNMT3B* is affected by Zn supports our above result that methionine and Zn metabolism are interdependent.

We previously reported that PSCs maintained their intracellular SAM level for a short time under (−) Met conditions by activating the MTA pathway, increasing *MAT2A*, or decreasing *DNMT3B* transcripts (Shiraki et al., 2014). The altered methionine metabolism metabolites by (−) Zn appear to trigger the changes in the *MAT2A* and *DNMT3B* transcripts. This adaptation seems to occur under the present (−) Zn condition.

INS and IGF signaling in stem cells and endocrine β cell differentiation

INS/IGF1 signaling pathways are present in most cells and mediate essential roles in the growth and metabolism of tissues. IGF1/INS signaling is implicated in sustaining pluripotency or promoting stem cell proliferation and plays a role in differentiation (Anderson et al., 2017; Chen and Khillan, 2010; Freund et al., 2008; Gupta et al., 2018; Huang et al., 2009; Li and Geng, 2010). INS is often used as a supplement to maintain hiPSC growth. INS forms a hexamer complex in the presence of Zn. To establish a culture system without Zn, we explored the possibility of substituting INS with IGF1. Our results confirmed that INS could be replaced by IGF1, at least in the short term, to maintain the pluripotency of hiPSCs. Our results also shed light on the importance of INS as a supply for Zn that contributes to sustaining cell growth and pluripotency, which serves as a barrier to inducing differentiation. Therefore, removing INS and Zn from the differentiation media potentiates endoderm differentiation.

Using IGF1 as a growth factor supplement, we found that IGF1 could sustain differentiation into DE and PP cells. However, upon culture extension, the IGF1 supplementation condition resulted in a marked decrease in cell number observed from stage S4. Reduced differentiation into β cells was not observed, but cell survival was decreased. We then explored the mechanism that reduces cell number in late-stage differentiation into endocrine β cells. INS* was added to the culture, which rescued cell survival. Previous reports suggested that signaling through insulin or the IGF1 receptor is not crucial for early β cell development. In the β cell-specific insulin receptor or the IGF1 receptor knockout mice (Kulkarni et al., 1999, 2002), double-mutant mice are born with normal islets or β cells (Ueki et al., 2006). Our result suggests that IGF1 is insufficient for cell survival in our present differentiation system. INS signaling seems indispensable for cell survival during β cell differentiation from hiPSCs. IGF1 signaling is regulated by binding partners, such as IGF-binding proteins (IGFBPs) (Bach, 2018; Miyamoto et al., 2004). Several members of IGFBPs were expressed at stage S5 (E.Z.S. and N.S., et al., unpublished data).

Recent reports show the generation of functional pancreatic β cells from hESCs/iPSCs in basal media containing low Zn and insulin concentrations for endoderm differentiation (Pagliuca et al., 2014; Velazco-Cruz et al., 2019; Veres et al., 2019). These reports concur with our finding that low Zn conditions potentiate the differentiation of hiPSCs.

Zn signaling in sustaining cell proliferation of iPSCs and its role in pancreatic differentiation

We found that Zn is essential for cell proliferation in hiPSCs, which is in line with our observation that increasing Zn concentration downregulates genes involved in regulating autophagy, actin filaments, and cellular response to starvation. A report that $ZnCl_2$ transiently maintained the pluripotency of mouse ESCs *in vitro* in the absence of leukemia inhibitory factor (LIF) agrees with our observation (Hu et al., 2016).

Our results show that the differentiation of iPSCs into DE at (−) Zn conditions led to a decreased proportion of OCT3/4$^+$ cells, potentiating differentiation into the pancreatic β cells. We also found that a moderate Zn concentration of 3 μM is beneficial for efficient differentiation into pancreatic progenitor cells and further into endocrine cells (S3–S5). The requirement for Zn in the culture may result from the demand for different Zn-binding proteins that function during β cell differentiation. The expression of *SLC30A8* is detected at stage 6, which may explain the requirement of a high Zn concentration at 10 μM during late stages. *SLC30A8* encoding ZNT8 is reported to transport Zn into the INS secretory granules, where a high level of Zn is required for the crystallization of INS through the binding of six INS monomers to two Zn ions (Emdin et al., 1980; Rutter and Chimienti, 2015; Vinkenborg et al., 2009). *SLC30A8* is a risk factor for type 2 diabetes, as reported in genome-wide association studies (Rutter and Chimienti, 2015; Sladek et al., 2007). Null or β cell-specific *Slc30a8* deletion mutants have shown defects in Zn-INS crystal formation (Halloran et al., 2013; Lemaire et al., 2009; Nicolson et al., 2009; Wijesekara et al., 2010).

We previously reported the intracellular Zn contents during cellular differentiation from iPSCs to pancreatic β cells using high-performance liquid chromatography (HPLC) coupled to inductively coupled plasma mass spectrometry (ICP-MS) (Arakawa et al., 2016). The hiPSCs contained the highest protein-binding Zn at approximately 17 ng/10^6 cells, which decreased

Figure 7. Exogenous HCY substitutes Zn to decrease protein-bound Zn in hiPSCs and changes in metabolites involved in methionine metabolism in response to Zn deprival

(A and B) Intracellular (A) and extracellular (B) contents of the metabolites involved in methionine metabolism at (−) Zn (closed circle) or 3 μM Zn (open circle). Ff-I01s01 human iPSCs were cultured under a custom-developed medium AKM (IGF1) at (−) Zn or 3 μM Zn for 2–3 days. The extracellular metabolites presented are calculated as follows: The measurements were subtracted with the initial amounts of the metabolites existing in the fresh medium and were normalized to 24 h with the cell number (nmol/24 h/1 × 10^6 cells). (−) values: Consumption by the cells, (+) values: excretion from the cells. A 2-tailed paired t test analyzed differences between groups, shown as *p < 0.05, **p < 0.01, and ***p < 0.001. ns, not significant. Detailed methods are provided in Method details.

at DE, PP, and EC stages to approximately 6–8 ng/10^6 cells. Interestingly, the amount of labile Zn is the highest at approximately 0.6 ng/10^6 cells at the EC stage (Arakawa et al., 2016). Undifferentiated iPSCs show an increased requirement for Zn to maintain their pluripotency and cell proliferation.

The effect of (−) Met is rapid, and long-term deprival triggers the apoptosis of hiPSCs. By contrast, the impact of (−) Zn is slow and does not trigger the apoptosis of hiPSCs. Treatment of hiPSCs under (−) Zn was done under conditions that methionine is supplied from the medium, thereby minimizing the toxic effects. Nevertheless, methionine metabolism-related metabolites are affected under the (−) Zn condition. Combining (−) Met and (−) Zn may be a valuable strategy for differentiating hiPSCs into endodermal lineages. The iPSCs contain high Zn-binding proteins that store and provide Zn. The contents of the Zn-binding proteins in the hiPSCs may vary depending on the extent of cell growth or differentiation state, which may explain why (−) Zn potentiated differentiation into endoderm but not mesoderm or ectoderm.

We found that lowering intracellular Zn is one of the (−) Met downstream targets. Long-term (−) Met treatment triggers the apoptosis of PSCs. We adopted a short-term (−) Met protocol to enhance differentiation. This protocol is applicable for many different cell lines to establish a robust differentiation protocol by controlling the nutrition. To bypass the toxic effects of (−) Met by prolonged treatment, we performed (−) Met treatment, followed by (−) Zn treatment during DE differentiation, which effectively eliminated undifferentiated cells during early stages, thereby enhancing late-stage differentiation.

Limitations of the study

We have shown that (−) Met decreased protein-bound Zn through an increased intracellular local HCY. However, the intracellular HCY was under the detectable range. There is a limitation in the present techniques to detect the low amount of intracellular HCY and its subcellular localization.

STAR★METHODS

Detailed methods are provided in the online version of this paper and include the following:

- KEY RESOURCES TABLE
- RESOURCE AVAILABILITY
  - Lead contact
  - Material availability
  - Data and code availability
- EXPERIMENTAL MODEL AND SUBJECT DETAILS
  - Ethical approval
  - Human iPS and ES cell lines
  - Primary human islets and human islet cDNA
- METHOD DETAILS
  - Maintenance culture of hiPSCs and hESCs
  - Medium
  - Single amino acid deprivation
  - Zn deprivation using chelex 100
  - Analysis of Zn and other metal content
  - HCY treatment of cell lysates from hiPSCs
  - Western blot analysis for ZnT1
  - Knockdown of *SLC30A1* using siRNA
  - EdU incorporation
  - TUNEL analysis
  - Alkaline phosphatase staining
  - Assessment of extracellular ATP content
  - Sphere formation and methionine deprivation
  - Pancreatic differentiation protocol in Figure 1
  - Pretreatment of hiPSCs with AKM (Zn 0 / IGF)
  - Mesoderm and ectoderm differentiation using AKM media
  - Endoderm differentiation using AKM media
  - Pancreatic differentiation using AKM medium
  - Pancreatic differentiation using MCDB medium
  - Immunocytochemistry
  - Real-time PCR analysis
  - Affymetrix microarray analysis and accession numbers
  - RNA sequencing
  - Principal component analysis
  - Reaggregation of hiPSβ
  - C-peptide release and content assay
  - Dynamic GSIS
  - Metabolite analysis
- QUANTIFICATION AND STATISTICAL ANALYSIS

SUPPLEMENTAL INFORMATION

Supplemental information can be found online at https://doi.org/10.1016/j.celrep.2022.111120.

ACKNOWLEDGMENTS

We thank the members of the Center for Biological Resources and the Open Research Facilities for Life Science and Technology at the Tokyo Institute of Technology for their technical assistance. This work was supported by a grant from the Project for Realization of Regenerative Medicine (to S.K.) from the Japan Agency for Medical Research and Development (AMED). This work was also supported partly by Grants-in-Aid from the Ministry of Education, Culture, Sports, Science and Technology (MEXT) Japan [#21H02978 to S.K., #18H02154 to N.S., and 21H04774 to M.M.). This work was also supported in part by the Danone Institute research project (to N.S.), the Takeda Science Foundation (to S.K.), and the Japanese Insulin Dependent Diabetes Mellitus (IDDM) Network Foundation.

AUTHOR CONTRIBUTIONS

E.Z.S., T.E., and N.S. designed the experiments and acquired, analyzed, and interpreted the data. N.F., S.K., T.T., A.A., and M.Y. designed, acquired, and analyzed part of the experiments. H.O. analyzed and discussed the data. T.K. and M.M. discussed the data. N.S. and S.K. provided conceptual input, discussion, writing, and revision of the manuscript; approved the final version of the manuscript; and obtained funding.

DECLARATION OF INTERESTS

A part of the research was conducted with a research fund from Ajinomoto. A.A., H.O., and M.Y. are salaried employees of Ajinomoto. A part of the research is related to a patent that is pending.

Received: July 21, 2020
Revised: April 19, 2022
Accepted: June 28, 2022
Published: July 19, 2022

REFERENCES

Abdel-Azeim, S., Li, X., Chung, L.W., and Morokuma, K. (2011). Zinc-Homocysteine binding in cobalamin-dependent methionine synthase and its role in the substrate activation: DFT, ONIOM, and QM/MM molecular dynamics studies. J. Comput. Chem. *32*, 3154–3167.

Anderson, K.G.V., Hamilton, W.B., Roske, F.V., Azad, A., Knudsen, T.E., Canham, M., Forrester, L.M., and Brickman, J.M. (2017). Insulin fine-tunes self-renewal pathways governing naive pluripotency and extra-embryonic endoderm. Nat. Cell Biol. *19*, 1164–1177. https://doi.org/10.1038/ncb3617.

Andreini, C., Banci, L., Bertini, I., Rosato, A., et al. (2006). Counting the Zinc-Proteins Encoded in the Human Genome. Journal of Proteome Research *5*, 196–201. https://doi.org/10.1021/pr050361j.

Andrews, G.K., Wang, H., Dey, S.K., and Palmiter, R.D. (2004). Mouse zinc transporter 1 gene provides an essential function during early embryonic development. Genesis *40*, 74–81. https://doi.org/10.1002/gene.20067.

Anzellotti, A.I., and Farrell, N.P. (2008). Zinc metalloproteins as medicinal targets. Chem. Soc. Rev. *37*, 1629. https://doi.org/10.1039/b617121b.

Arakawa, A., Shiraki, N., Tsuyama, T., Kume, S., Iwahata, D., and Yamada, N. (2016). Analytical & bioanalytical speciation of intracellular Zn, Fe and Cu within both iPS cells and differentiated cells using HPLC coupled to ICP-MS. Anal. Bioanal. Tech. *7*, 1–8.

Bach, L.A. (2018). 40 years of IGF1: IGF-binding proteins. J. Mol. Endocrinol. *61*, T11–T28. https://doi.org/10.1530/jme-17-0254.

Becker, R.H. (2007). Insulin glulisine complementing basal insulins: a review of structure and activity. Diabetes Technol. Ther. *9*, 109–121. https://doi.org/10.1089/dia.2006.0035.

Brange, J., Havelund, S., Hommel, E., Sørensen, E., and Kühl, C. (1986). Neutral insulin solutions physically stabilized by addition of Zn 2+. Diabet. Med. *3*, 532–536. https://doi.org/10.1111/j.1464-5491.1986.tb00809.x.

Chen, L., and Khillan, J.S. (2010). A novel signaling by vitamin A/retinol promotes self renewal of mouse embryonic stem cells by activating PI3K/Akt signaling pathway via insulin-like growth factor-1 receptor. Stem Cell. *28*, 57–63. https://doi.org/10.1002/stem.251.

Choi, S., and Bird, A.J. (2014). Zinc'ing sensibly: controlling zinc homeostasis at the transcriptional level. Metallomics *6*, 1198–1215. https://doi.org/10.1039/c4mt00064a.

Danchin, A. (2020). Zinc, an unexpected integrator of metabolism? Microb. Biotechnol. *13*, 895–898.

Emdin, S.O., Dodson, G.G., Cutfield, J.M., and Cutfield, S.M. (1980). Role of zinc in insulin biosynthesis - some possible zinc-insulin interactions in the pancreatic B-cell. Diabetologia *19*, 174–182. https://doi.org/10.1007/bf00275265.

Evans, J.C., Huddler, D.P., Jiracek, J., Castro, C., Millian, N.S., Garrow, T.A., and Ludwig, M.L. (2002). Betaine-homocysteine methyltransferase. Structure *10*, 1159–1171. https://doi.org/10.1016/s0969-2126(02)00796-7.

Freund, C., Ward-van Oostwaard, D., Monshouwer-Kloots, J., van den Brink, S., van Rooijen, M., Xu, X., Zweigerdt, R., Mummery, C., and Passier, R. (2008). Insulin redirects differentiation from cardiogenic mesoderm and endoderm to neuroectoderm in differentiating human embryonic stem cells. Stem Cell. *26*, 724–733. https://doi.org/10.1634/stemcells.2007-0617.

Fukada, T., Yamasaki, S., Nishida, K., Murakami, M., and Hirano, T. (2011). Zinc homeostasis and signaling in health and diseases: zinc signaling. J. Biol. Inorg. Chem. *16*, 1123–1134. https://doi.org/10.1007/s00775-011-0797-4.

Gamble, A., Pepper, A.R., Bruni, A., and Shapiro, A.M.J. (2018). The journey of islet cell transplantation and future development. Islets *10*, 80–94. https://doi.org/10.1080/19382014.2018.1428511.

Gonzalez-Iglesias, H., Alvarez, L., García, M., Petrash, C., Sanz-Medel, A., and Coca-Prados, M. (2014). Metallothioneins (MTs) in the human eye: a perspective article on the zinc–MT redox cycle. Metallomics *6*, 201. https://doi.org/10.1039/c3mt00298e.

González, B., Pajares, M.A., Martínez-Ripoll, M., Blundell, T.L., and Sanz-Aparicio, J. (2004). Crystal structure of rat liver betaine homocysteine S-methyltransferase reveals new oligomerization features and conformational changes upon substrate binding. J. Mol. Biol. *338*, 771–782. https://doi.org/10.1016/j.jmb.2004.03.005.

Gupta, M.K., De Jesus, D.F., Kahraman, S., Valdez, I.A., Shamsi, F., Yi, L., Swensen, A.C., Tseng, Y.H., Qian, W.J., and Kulkarni, R.N. (2018). Insulin receptor-mediated signaling regulates pluripotency markers and lineage differentiation. Mol. Metab. *18*, 153–163. https://doi.org/10.1016/j.molmet.2018.09.003.

Halloran, T.V.O., Philips, S.J., and Attie, A.D. (2013). Zinc, insulin, and the liver: a ménage à trois. J. Clin. Investig. *123*, 4136–4139.

Hardyman, J.E.J., Tyson, J., Jackson, K.A., Aldridge, C., Cockell, S.J., Wakeling, L.A., Valentine, R.A., and Ford, D. (2016). Zinc sensing by metal-responsive transcription factor 1 (MTF1) controls metallothionein and ZnT1 expression to buffer the sensitivity of the transcriptome response to zinc. Metallomics *8*, 337–343. https://doi.org/10.1039/c5mt00305a.

Hensley, M.P., Tierney, D.L., and Crowder, M.W. (2011). Zn(II) binding to Escherichia coli 70S ribosomes. Biochemistry *50*, 9937–9939. https://doi.org/10.1021/bi200619w.

Hensley, M.P., Gunasekera, T.S., Easton, J.A., Sigdel, T.K., Sugarbaker, S.A., Klingbeil, L., Breece, R.M., Tierney, D.L., and Crowder, M.W. (2012). Characterization of Zn(II)-responsive ribosomal proteins YkgM and L31 in E. coli. J. Inorg. Biochem. *111*, 164–172. https://doi.org/10.1016/j.jinorgbio.2011.11.022.

Ho, M.C.D., Ring, N., Amaral, K., Doshi, U., and Li, A.P. (2017). Human enterocytes as an in vitro model for the evaluation of intestinal drug metabolism: characterization of drug-metabolizing enzyme activities of cryopreserved human enterocytes from twenty-four donors. Drug Metab. Dispos. *45*, 686–691. https://doi.org/10.1124/dmd.116.074377.

Hu, J., Yang, Z., Wang, J., Yu, J., Guo, J., Liu, S., Qian, C., Song, L., Wu, Y., and Cheng, J. (2016). Zinc chloride transiently maintains mouse embryonic stem cell pluripotency by activating Stat3 signaling. PLoS One *11*, e0148994. https://doi.org/10.1371/journal.pone.0148994.

Huang, Y.-H., Chin, C.-C., Ho, H.-N., Chou, C.-K., Shen, C.-N., Kuo, H.-C., Wu, T.-J., Wu, Y.-C., Hung, Y.-C., Chang, C.-C., and Ling, T.Y. (2009). Pluripotency of mouse spermatogonial stem cells maintained by IGF-1-dependent pathway. FASEB J. *23*, 2076–2087. https://doi.org/10.1096/fj.08-121939.

Inoue, H., Nagata, N., Kurokawa, H., and Yamanaka, S. (2014). iPS cells: a game changer for future medicine. EMBO J. *33*, 409–417. https://doi.org/10.1002/embj.201387098.

Jiang, Z., Liang, Q., Luo, G., Hu, P., Li, P., and Wang, Y. (2009). HPLC-electrospray tandem mass spectrometry for simultaneous quantitation of eight plasma aminothiols: Application to studies of diabetic nephropathy. Talanta *77*, 1279–1284. https://doi.org/10.1016/j.talanta.2008.08.031.

Kambe, T. (2019). Metalation and maturation of zinc ectoenzymes: a perspective. Biochemistry *59*, 74–79. https://doi.org/10.1021/acs.biochem.9b00924.

Kambe, T., Hashimoto, A., and Fujimoto, S. (2014). Current understanding of ZIP and ZnT zinc transporters in human health and diseases. Cell. Mol. Life Sci. *71*, 3281–3295. https://doi.org/10.1007/s00018-014-1617-0.

Kambe, T., Matsunaga, M., and Takeda, T.A. (2017). Understanding the contribution of zinc transporters in the function of the early secretory pathway. Int. J. Mol. Sci. *18*, 2179. https://doi.org/10.3390/ijms18102179.

Kieffer, T.J., Woltjen, K., Osafune, K., Yabe, D., and Inagaki, N. (2017). Beta cell replacement strategies for diabetes. J. Diabetes Investig. *9*, 457–463.

Kimura, T., and Kambe, T. (2016). The functions of metallothionein and ZIP and ZnT transporters: an overview and perspective. Int. J. Mol. Sci. *17*, 336. https://doi.org/10.3390/ijms17030336.

Koutmos, M., Pejchal, R., Bomer, T.M., Matthews, R.G., Smith, J.L., and Ludwig, M.L. (2008). Metal active site elasticity linked to activation of homocysteine in methionine synthases. Proc. Natl. Acad. Sci. USA *105*, 3286–3291. https://doi.org/10.1073/pnas.0709960105.

Krężel, A., and Maret, W. (2017). The functions of metamorphic metallothioneins in zinc and copper metabolism. Int. J. Mol. Sci. *18*, 1237. https://doi.org/10.3390/ijms18061237.

Kulkarni, R.N., Brüning, J.C., Winnay, J.N., Postic, C., Magnuson, M.A., and Kahn, C. (1999). Tissue-specific knockout of the insulin receptor in pancreatic β cells creates an insulin secretory defect similar to that in type 2 diabetes. Cell *96*, 329–339. https://doi.org/10.1016/s0092-8674(00)80546-2.

Kulkarni, R.N., Holzenberger, M., Shih, D.Q., Ozcan, U., Stoffel, M., Magnuson, M.A., and Kahn, C.R. (2002). β-cell-specific deletion of the Igf1 receptor leads to hyperinsulinemia and glucose intolerance but does not alter β-cell mass. Nat. Genet. *31*, 111–115. https://doi.org/10.1038/ng872.

Lemaire, K., Ravier, M.A., Schraenen, A., Creemers, J.W.M., Van De Plas, R., Granvik, M., Van Lommel, L., Waelkens, E., Chimienti, F., Rutter, G.A., et al. (2009). Insulin crystallization depends on zinc transporter ZnT8 expression, but is not required for normal glucose homeostasis in mice. Proc. Natl. Acad. Sci. USA *106*, 14872–14877. https://doi.org/10.1073/pnas.0906587106.

Li, Y., and Geng, Y.J. (2010). A potential role for insulin-like growth factor signaling in induction of pluripotent stem cell formation. Growth Horm. IGF Res. *20*, 391–398. https://doi.org/10.1016/j.ghir.2010.09.005.

Luo, C., Zhao, S., Zhang, M., Gao, Y., Wang, J., Hanigan, M.D., and Zheng, N. (2018). SESN2 negatively regulates cell proliferation and casein synthesis by inhibition the amino acid-mediated mTORC1 pathway in cow mammary epithelial cells. Sci. Rep. *8*, 3912. https://doi.org/10.1038/s41598-018-22208-w.

Martins, T.M.d.M., de Paula, A.C.C., Gomes, D.A., and Goes, A.M. (2014). Alkaline phosphatase expression/activity and multilineage differentiation potential are the differences between fibroblasts and orbital fat-derived stem cells – a study in animal serum-free culture conditions. Stem Cell Rev. Rep. *10*, 697–711. https://doi.org/10.1007/s12015-014-9529-9.

Millman, J.R., Xie, C., Van Dervort, A., Gürtler, M., Pagliuca, F.W., and Melton, D.A. (2016). Generation of stem cell-derived β-cells from patients with type 1 diabetes. Nat. Commun. *7*, 11463. https://doi.org/10.1038/ncomms11463.

Miyamoto, S., Yano, K., Sugimoto, S., Ishii, G., Hasebe, T., Endoh, Y., Kodama, K., Goya, M., Chiba, T., and Ochiai, A. (2004). Matrix metalloproteinase-7 facilitates insulin-like growth factor bioavailability through its proteinase activity on insulin-like growth factor binding protein 3. Cancer Res. *64*, 665–671. https://doi.org/10.1158/0008-5472.can-03-1916.

Nair, G.G., Liu, J.S., Russ, H.A., Tran, S., Saxton, M.S., Chen, R., Juang, C., Li, M.l., Nguyen, V.Q., Giacometti, S., et al. (2019). Recapitulating endocrine cell clustering in culture promotes maturation of human stem-cell-derived β cells. Nat. Cell Biol. *21*, 263–274. https://doi.org/10.1038/s41556-018-0271-4.

Nakashima, R., Morooka, M., Shiraki, N., Sakano, D., Ogaki, S., Kume, K., and Kume, S. (2015). Neural cells play an inhibitory role in pancreatic differentiation of pluripotent stem cells. Gene Cell. *20*, 1028–1045. https://doi.org/10.1111/gtc.12308.

Nicolson, T.J., Bellomo, E.A., Wijesekara, N., Loder, M.K., Baldwin, J.M., Gyulkhandanyan, A.V., Koshkin, V., Tarasov, A.I., Carzaniga, R., Kronenberger, K., et al. (2009). Insulin storage and glucose homeostasis in mice null for the granule zinc transporter ZnT8 and studies of the type 2 diabetes-associated variants. Diabetes *58*, 2070–2083. https://doi.org/10.2337/db09-0551.

Nishito, Y., and Kambe, T. (2019). Zinc transporter 1 (ZNT1) expression on the cell surface is elaborately controlled by cellular zinc levels. J. Biol. Chem. *294*, 15686–15697. https://doi.org/10.1074/jbc.ra119.010227.

Nishito, Y., Tsuji, N., Fujishiro, H., Takeda, T.A., Yamazaki, T., Teranishi, F., Okazaki, F., Matsunaga, A., Tuschl, K., Rao, R., et al. (2016). Direct comparison of manganese detoxification/efflux proteins and molecular characterization of ZnT10 protein as a manganese transporter. J. Biol. Chem. *291*, 14773–14787. https://doi.org/10.1074/jbc.m116.728014.

Nishizawa, M., Chonabayashi, K., Nomura, M., Tanaka, A., Nakamura, M., Inagaki, A., Nishikawa, M., Takei, I., Oishi, A., Tanabe, K., et al. (2016). Epigenetic variation between human induced pluripotent stem cell lines is an indicator of differentiation capacity. Cell Stem Cell *19*, 341–354. https://doi.org/10.1016/j.stem.2016.06.019.

Osafune, K., Caron, L., Borowiak, M., Martinez, R.J., Fitz-Gerald, C.S., Sato, Y., Cowan, C.A., Chien, K.R., and Melton, D.A. (2008). Marked differences in differentiation propensity among human embryonic stem cell lines. Nat. Biotechnol. *26*, 313–315. https://doi.org/10.1038/nbt1383.

Pagliuca, F., Millman, J., Gürtler, M., Segel, M., Van Dervort, A., Ryu, J., Peterson, Q., Greiner, D., and Melton, D. (2014). Generation of functional human pancreatic β cells in vitro. Cell *159*, 428–439. https://doi.org/10.1016/j.cell.2014.09.040.

Qi, Y., Zhang, X.J., Renier, N., Wu, Z., Atkin, T., Sun, Z., Ozair, M.Z., Tchieu, J., Zimmer, B., Fattahi, F., et al. (2017). Combined small-molecule inhibition accelerates the derivation of functional cortical neurons from human pluripotent stem cells. Nat. Biotechnol. *35*, 154–163. https://doi.org/10.1038/nbt.3777.

Rezania, A., Bruin, J.E., Arora, P., Rubin, A., Batushansky, I., Asadi, A., O'Dwyer, S., Quiskamp, N., Mojibian, M., Albrecht, T., et al. (2014). Reversal of diabetes with insulin-producing cells derived in vitro from human pluripotent stem cells. Nat. Biotechnol. *32*, 1121–1133. https://doi.org/10.1038/nbt.3033.

Russ, H.A., Parent, A.V., Ringler, J.J., Hennings, T.G., Nair, G.G., Shveygert, M., Guo, T., Puri, S., Haataja, L., Cirulli, V., et al. (2015). Controlled induction of human pancreatic progenitors produces functional beta-like cells *in vitro*. EMBO J. *34*, 1759–1772. https://doi.org/10.15252/embj.201591058.

Rutter, G.a., and Chimienti, F. (2015). SLC30A8 mutations in type 2 diabetes. Diabetologia *58*, 31–36. https://doi.org/10.1007/s00125-014-3405-7.

Sakano, D., Shiraki, N., Kikawa, K., Yamazoe, T., Kataoka, M., Umeda, K., Araki, K., Mao, D., Matsumoto, S., Nakagata, N., Andersson, O., Stainier, D., Endo, F., Kume, K., Uesugi, M., Kume, S., et al. (2014). VMAT2 identified as a regulator of late-stage β-cell differentiation. Nature Chemical Biology *10*, 141–148. https://doi.org/10.1038/nchembio.1410.

Sánchez Alvarado, A., and Yamanaka, S. (2014). Rethinking differentiation: stem cells, regeneration, and plasticity. Cell *157*, 110–119. https://doi.org/10.1016/j.cell.2014.02.041.

Shahjalal, H.M., Shiraki, N., Sakano, D., Kikawa, K., Ogaki, S., Baba, H., Kume, K., and Kume, S. (2014). Generation of insulin-producing β-like cells from human iPS cells in a defined and completely xeno-free culture system. J. Mol. Cell Biol. *6*, 394–408.

Shapiro, A.M.J., Pokrywczynska, M., and Ricordi, C. (2017). Clinical pancreatic islet transplantation. Nat. Rev. Endocrinol. *13*, 268–277. https://doi.org/10.1038/nrendo.2016.178.

Shiraki, N., Shiraki, Y., Tsuyama, T., Obata, F., Miura, M., Nagae, G., Aburatani, H., Kume, K., Endo, F., and Kume, S. (2014). Methionine metabolism regulates maintenance and differentiation of human pluripotent stem cells. Cell Metabol. *19*, 780–794. https://doi.org/10.1016/j.cmet.2014.03.017.

Shyh-Chang, N., Locasale, J.W., Lyssiotis, C.A., Zheng, Y., Teo, R.Y., Ratanasirintrawoot, S., Zhang, J., Onder, T., Unternaehrer, J.J., Zhu, H., et al. (2013). Influence of threonine metabolism on S -adenosylmethionine and histone methylation. Science *339*, 222–226. https://doi.org/10.1126/science.1226603.

Sladek, R., Rocheleau, G., Rung, J., Dina, C., Shen, L., Serre, D., Boutin, P., Vincent, D., Belisle, A., Hadjadj, S., et al. (2007). A genome-wide association study identifies novel risk loci for type 2 diabetes. Nature *445*, 881–885. https://doi.org/10.1038/nature05616.

Suemori, H., Yasuchika, K., Hasegawa, K., Fujioka, T., Tsuneyoshi, N., and Nakatsuji, N. (2006). Efficient establishment of human embryonic stem cell lines and long-term maintenance with stable karyotype by enzymatic bulk passage. Biochem. Biophys. Res. Commun. *345*, 926–932. https://doi.org/10.1016/j.bbrc.2006.04.135.

Sugita, S., Iwasaki, Y., Makabe, K., Kimura, T., Futagami, T., Suegami, S., and Takahashi, M. (2016). Lack of T Cell response to iPSC-derived retinal pigment epithelial cells from HLA homozygous donors. Stem Cell Rep. *7*, 619–634. https://doi.org/10.1016/j.stemcr.2016.08.011.

Suzuki, T., Ishihara, K., Migaki, H., Matsuura, W., Kohda, A., Okumura, K., Nagao, M., Yamaguchi-Iwai, Y., and Kambe, T. (2005). Zinc transporters, ZnT5 and ZnT7, are required for the activation of alkaline phosphatases, zinc-requiring enzymes that are glycosylphosphatidylinositol-anchored to the

cytoplasmic membrane. J. Biol. Chem. *280*, 637–643. https://doi.org/10.1074/jbc.m411247200.

Takahashi, K., and Yamanaka, S. (2016). A decade of transcription factor-mediated reprogramming to pluripotency. Nat. Rev. Mol. Cell Biol. *17*, 183–193. https://doi.org/10.1038/nrm.2016.8.

Takahashi, K., Tanabe, K., Ohnuki, M., Narita, M., Ichisaka, T., Tomoda, K., and Yamanaka, S. (2007). Induction of pluripotent stem cells from adult human fibroblasts by defined factors. Cell *131*, 861–872. https://doi.org/10.1016/j.cell.2007.11.019.

Takebe, T., Sekine, K., Kimura, M., Yoshizawa, E., Ayano, S., Koido, M., Funayama, S., Nakanishi, N., Hisai, T., Kobayashi, T., et al. (2017). Massive and reproducible production of liver buds entirely from human pluripotent stem cells. Cell Rep. *21*, 2661–2670. https://doi.org/10.1016/j.celrep.2017.11.005.

Takeda, T.a., Miyazaki, S., Kobayashi, M., Nishino, K., Goto, T., Matsunaga, M., Ooi, M., Shirakawa, H., Tani, F., Kawamura, T., et al. (2018). Zinc deficiency causes delayed ATP clearance and adenosine generation in rats and cell culture models. Commun. Biol. *1*, 113. https://doi.org/10.1038/s42003-018-0118-3.

Thomson, J.A., Itskovitz-eldor, J., Shapiro, S.S., Waknitz, M.A., Swiergiel, J.J., Marshall, V.S., Jones, J.M., Thomson, J.A., Joseph Itskovitz-Eldor, S.S.S., Waknitz, M.A., et al. (1998). Embryonic stem cell lines derived from human blastocysts. Science *282*, 1145–1147. https://doi.org/10.1126/science.282.5391.1145.

Ueki, K., Okada, T., Hu, J., Liew, C.W., Assmann, A., Dahlgren, G.M., Peters, J.L., Shackman, J.G., Zhang, M., Artner, I., et al. (2006). Total insulin and IGF-I resistance in pancreatic β cells causes overt diabetes. Nat. Genet. *38*, 583–588. https://doi.org/10.1038/ng1787.

Velazco-Cruz, L., Song, J., Maxwell, K.G., Goedegebuure, M.M., Augsornworawat, P., Hogrebe, N.J., and Millman, J.R. (2019). Acquisition of dynamic function in human stem cell-derived β cells. Stem Cell Rep. *12*, 351–365. https://doi.org/10.1016/j.stemcr.2018.12.012.

Veres, A., Faust, A.L., Bushnell, H.L., Engquist, E.N., Kenty, J.H.-R., Harb, G., Poh, Y.-C., Sintov, E., Gürtler, M., Pagliuca, F.W., et al. (2019). Charting cellular identity during human in vitro β-cell differentiation. Nature *569*, 368–373. https://doi.org/10.1038/s41586-019-1168-5.

Vieira, A., Druelle, N., Avolio, F., Napolitano, T., Navarro-Sanz, S., Silvano, S., and Collombat, P. (2017). β-cell replacement strategies: the increasing need for a "β-cell dogma. Front. Genet. *8*, 75. https://doi.org/10.3389/fgene.2017.00075.

Vinkenborg, J.L., Nicolson, T.J., Bellomo, E.A., Koay, M.S., Rutter, G.A., and Merkx, M. (2009). Genetically encoded FRET sensors to monitor intracellular Zn2+ homeostasis. Nat. Methods *6*, 737–740. https://doi.org/10.1038/nmeth.1368.

Wang, J., Alexander, P., Wu, L., Hammer, R., Cleaver, O., and McKnight, S.L. (2009). Dependence of mouse embryonic stem cells on threonine catabolism. Science *325*, 435–439. https://doi.org/10.1126/science.1173288.

Wijesekara, N., Dai, F.F., Hardy, A.B., Giglou, P.R., Bhattacharjee, A., Koshkin, V., Chimienti, F., Gaisano, H.Y., Rutter, G.A., and Wheeler, M.B. (2010). Beta cell-specific Znt8 deletion in mice causes marked defects in insulin processing, crystallisation and secretion. Diabetologia *53*, 1656–1668. https://doi.org/10.1007/s00125-010-1733-9.

Wu, J., Ocampo, A., and Belmonte, J.C.I. (2016). Cellular metabolism and induced pluripotency. Cell *166*, 1371–1385. https://doi.org/10.1016/j.cell.2016.08.008.

Yamasaki, S., Sakata-Sogawa, K., Hasegawa, A., Suzuki, T., Kabu, K., Sato, E., Kurosaki, T., Yamashita, S., Tokunaga, M., Nishida, K., and Hirano, T. (2007). Zinc is a novel intracellular second messenger. J. Cell Biol. *177*, 637–645. https://doi.org/10.1083/jcb.200702081.

Yoshioka, N., Gros, E., Li, H.R., Kumar, S., Deacon, D., Maron, C., Muotri, A., Chi, N., Fu, X.D., Yu, B., and Dowdy, S. (2013). Efficient generation of human iPSCs by a synthetic self-replicative RNA. Cell Stem Cell *13*, 246–254. https://doi.org/10.1016/j.stem.2013.06.001.

Zhu, S., Russ, H.A., Wang, X., Zhang, M., Ma, T., Xu, T., Tang, S., Hebrok, M., and Ding, S. (2016). Human pancreatic beta-like cells converted from fibroblasts. Nat. Commun. *7*, 10080. https://doi.org/10.1038/ncomms10080.

STAR★METHODS

KEY RESOURCES TABLE

REAGENT or RESOURCE	SOURCE	IDENTIFIER
Antibodies		
Mouse monoclonal anti-OCT3/4, clone C-10	Santa Cruz Biotechnology	sc-5279; RRID: AB_628051
Goat anti-SOX17	R&D Systems	AF1924; RRID: AB_355060
Rabbit anti-SOX9	Merck	AB5535; RRID: AB_2239761
Goat anti-PDX1	R&D Systems	AF2419; RRID: AB_355257
Mouse monoclonal anti-NKX6.1	Developmental Studies Hybridoma Bank	F55A10; RRID: AB_532378
Guinea pig anti-Insulin	Agilent Dako	IR002; RRID: AB_2800361
Guinea pig anti-Insulin	Dako	A0564; RRID:AB_10013624
Rabbit anti-C-peptide	Cell Signaling Technology	4593; RRID: AB_10691857
Mouse monoclonal anti-Glucagon	Sigma-Aldrich	G2654; RRID: AB_259852
Rabbit anti-Somatostatin	Sigma-Aldrich	SAB4502861; RRID: AB_10747468
Mouse monoclonal anti-hZnT1	Dr. T. Kambe (Kyoto University)	Nishito et al., 2016
Rabbit monoclonal anti-β-Actin	Cell Signaling Technology	8457; RRID: AB_10950489
Chemicals, peptides, and recombinant proteins		
Activin A	Cell Guidance Systems	GFH6
B27 insulin supplement	Life Technologies	17504001
Insulin glulisine	Sanofi S.A.	Apidra
CHIR99021	Stemgent	04-0004-10
CHIR99021	Wako	034-23103
SANT-1	Sigma	S4572-5MG
Recombinant human FGF10	Pepro Tech, Inc.	AF100-26
LDN193189	Sigma	SML0559
All-trans Retionic acid	Stemgent	04-0021
TGF-β type I receptor kinase inhibitor II	Wako	018-23023
(-)-Indolactam V	R&D Systems	3651
Exendin-4	Cell Sciences, Inc.	CRE117C
Nicotinamide	Sigma	N0636
N-acetyl-L-cysteine	Nacalai Tesque	00512-84
$ZnSO_4$	Sigma	Z0251-100G
IGF1	Cell Guidance Systems	GFH34AF
IGF1	Oriental Yeast	47063900
Y27632	Wako	251-00514
KGF	Fujifilm-Wako	116-00811
Vitamin C	Sigma	A4544
PdBU	LC laboratories	P4833
γ-Secretase Inhibitor XXI (GSXXI)	Sigma	565790-1MGCN
Betacellulin	Pepro Tech, Inc.	100-50
L-3,3′,5-Triiodothyronine	Sigma	T6397-1G
Heparin	Sigma	H3149-50KU
Humankine BMP-4 (Recombinant Human)	Proteintech	HZ-1045
SB431542	Calbiochem	301836-41-9
XAV939	Wako	247-00951
ON-TARGETplus Human SLC30A1 siRNA	Horizon Discovery	L-007522-01
ON-TARGETplus Non-targeting Control siRNA	Horizon Discovery	D-001810-01

(*Continued on next page*)

Continued

REAGENT or RESOURCE	SOURCE	IDENTIFIER
Opti-MEM Reduced Serum medium	Gibco	31985062
Critical commercial assays		
PrestoBlue™ Cell Viability Reagent	Invitrogen	A13261
PrimerArray® Embryonic Stem Cells	Takara Bio Inc.	#PH016
DharmaFECT 1 transfection reagent	Horizon Discovery	T-2001
Human C-peptide ELISA Kit	Mercodia	10-1136-01
Biological samples		
Cadaveric human Islets	Prodo labs	N/A
Human Islets (1st strand cDNAs)	Cosmo Bio Co. Ltd	N/A
Experimental models: Cell lines		
Toe	National Center for Child Health and Development	MRC-iPS-27
RPChiPS771	REPROCELL Inc.	N/A
HLA homozygote donor derived iPSCs (Ff-I01s01, Ff-I14s03, Ff-I01s04, Ff-I14s04, Ff-MH09s01, Ff-MH15s01, Ff-MH15s02, and Ff-MH23s01)	Center for iPS Cell Research and Application, Kyoto University (CiRA)	N/A
201B7	CiRA	HP S0063 (RIKEN)
KhES-3	Institute for Frontier Medical Sciences, Kyoto University	CVCL_B233
Oligonucleoties		
qPCR primers for Figures 2, 3, 5, S1–S6, see Table S7	This paper	N/A
Software		
PRISM 7	GraphPad	RRID: SCR_002798
BioRender	BioRender.com	RRID: SCR_018361
JMP	SAS Institute Inc	RRID:SCR_014242

RESOURCE AVAILABILITY

Lead contact

Further information and requests for resources should be directed to and will be fulfilled by the Lead Contact, Shoen Kume (skume@bio.titech.ac.jp).

Material availability

All unique/stabe reagents generated in this study are available from the lead contact.

Data and code availability

- The microarray and RNA-seq data generated during this study are available at Gene Expression Omnibus, National Center for Biotechnology Information (GEO-NCBI): (GSE151794, GSE151795, GSE152017).
- This paper does not report original code.
- Any additional information required to reanalyze the data reported in this paper is available from the lead contact upon request.

EXPERIMENTAL MODEL AND SUBJECT DETAILS

Ethical approval

The use of hiPSCs derived from HLA homozygote donors was approved by the institutional ethical committee involving human materials by the Tokyo Institute of Technology and Kyoto University.

Human iPS and ES cell lines

Toe human iPS cell (hiPSC) line was established by Toyoda M., Kiyokawa N., Okita H., Miyagawa Y., Akutsu H, and Umezawa A. in National Institute for Child Health and Development, Tokyo. RPChiPS771 cells, which were established using synthetic self-

replicative RNA (Yoshioka et al., 2013), were obtained from REPROCELL Inc. (Tokyo). 201B7, HLA homozygote donor-derived iPSCs, Ff-I01s01, Ff-I14s03, Ff-I01s04, Ff-I14s04, Ff-MH09s01, Ff-MH15s01, Ff-MH15s02, and Ff-MH23s01, were obtained from the Center for iPS Cell Research and Application, Kyoto University (CiRA). Human KhES3 (Suemori et al., 2006) was used, hESCs were approved by the Tokyo Institute of Technology's Institutional Review Board, following the hESC guidelines of the Japanese government.

Primary human islets and human islet cDNA

Non-diabetic human islets were obtained from Prodo Laboratories (HP17040-01, HP-18157-01, and HP-20003-01), cultured in Prodo Islet Medium (Prodo Laboratories), and used for glucose-stimulated C-peptide secretion analysis (Figure 5E). For human islet cDNA, RNA extracts from the above primary human islets (#HP-20003-01), and 3 batches of first strand cDNA from non-diabetic human islets (COSMO BIO Co. Ltd.): HIcDNA133, HIcDNA149, and HIcDNA171) were used in Figures 5 and S5. Detailed information is available at https://www.primarycell.com/hanbai/pancreatic_islets_cdna.html). RNA extracts from primary human islets (#HP-14341-01) were used for microarray analysis (Figure 1D).

METHOD DETAILS

Maintenance culture of hiPSCs and hESCs

Undifferentiated Toe, 201B7, RPChiPS771 hiPSCs, and KhES3 hESCs were maintained in StemFit AK02N media (Ajinomoto, Tokyo). HLA homozygote donor-derived iPSCs were maintained in StemFit AK03N. StemFit media were supplemented with Penicillin and Streptomycin. Human iPSCs and hESCs were freeze-thawed and cultured on a 100 mm CellBIND dish (Corning) pre-coated overnight with Synthemax II (Corning Cat No.3535) in maintenance media supplemented with 10 μM Y27632 (Wako Cat No.251-00514).

Medium

For the maintenance of undifferentiated iPSCs, bFGF was supplemented with StemFit media, such as AK02N, AK03N, a (-) Met medium (KA01), single amino acid deprived StemFit media, or AKM medium. AKM (INS) medium was INS and Zn containing media (StemFit Basic03). AKM (Zn0) medium was a (-) Zn basal medium (KA02, Ajinomoto, Inc., Tokyo). AKM (IGF1) medium was AKM (Zn0) medium + 100 ng/mL IGF1(Cell Guidance Systems or Oriental Yeast Co., Ltd.). AKM (INS*) medium was AKM (Zn0) medium + 19.4 μg/mL insulin glulisine (Sanofi SA), an insulin analog with no Zn binding sites. The concentration of insulin glulisine in AKM (INS*) is the same as that of INS in a chemically defined E8 medium (Chen and Khillan, 2010). HepG2 and HeLa cells were maintained in DMEM (Life Technologies) supplemented with 10% FBS (Hyclone) and Penicillin-Streptomycin (PS; Nacalai Tesque) and custom-made (-) Met medium (Funakoshi Co., Ltd.) was used for methionine deprivation.

Single amino acid deprivation

Custom-made StemFit KA01 media ((-) Met) or media deprived of single amino acid was used (Ajinomoto, Inc., Tokyo).

Zn deprivation using chelex 100

Chelex 100 resin was prewashed following the manufacturer's instructions (BioRad Laboratories). Human iPSC maintenance media StemFit AK medium (40 mL) was added to prewashed Chelex 100 resin (1.2g) and incubated for 2 h 45 min with rotation, filtered (0.22 μm filter), and the metals quantified by Ajinomoto Inc. Control complete media was prepared by replenishing all metals, $ZnSO_4.7H_2O$ (Sigma), $Fe(NO_3)_3.9H_2O$ (Wako, Tokyo), $CaCl_2$ (Nacalai Tesque, Kyoto), and $MgSO_4$ (SIGMA). Zn was excluded from the Zn deprived ((-) Zn) medium.

201B7 undifferentiated hiPSCs were dissociated and plated at $1x10^5$ cells/well on SynthemaxII-coated plates 6-well plates (Corning) and cultured at 37°C for 24 h. The cells were then washed with PBS (-) and with the medium replaced with (-) Zn or the control complete medium described above and cultured for 24, 48, or 72 h. The cells were then dissociated, counted, and harvested.

Analysis of Zn and other metal content

Intracellular free and protein-bound metal (Zn, Co, Fe, Mg, Ca) contents were measured using high-performance liquid chromatography (HPLC) coupled to inductively coupled plasma mass spectrometry (HPLC-ICP-MS) in Ajinomoto Co., Inc., as previously described (Arakawa et al., 2016). This method enables the separation of intracellular metal species into two types of chemical forms, namely, free ions and protein-bound metals, by their molecular size. After separation by HPLC, the separated aliquots were directly introduced to ICP-MS for quantification. The total heavy metal content in the medium was measured before and after Chelex 100 treatment and then replenished accordingly (except Zn for preparing (-) Zn medium).

HCY treatment of cell lysates from hiPSCs

201B7 iPSCs cultured for 5 h in complete medium or (-) Met medium for 5 h were harvested, and cell lysates were prepared as described (Arakawa et al., 2016). The lysates were added with HCY at 1, 5, 10, 50, 500, 1000, or 2000 μM and incubated for 2 h at 4°C. The contents of protein-bound metal (Zn, Cu, Fe) were then measured using the method described above.

Western blot analysis for ZnT1

Total protein extraction was performed with lysis buffer (10 mM Tris/HCl pH 7.5, 0.5 mM $MgCl_2$, and 0.1% Triton X-100) (Suzuki et al., 2005). Proteins were separated in 8% SDS-PAGE with Mini-PROTEAN Electrophoresis System (Bio-Rad) and transferred to a PVDF (Millipore) membrane by Trans-Blot Semi-Dry Transfer Cell (Bio-Rad). Membranes were then blocked with 5% skimmed milk in PBS-T and then incubated with primary antibodies overnight at 4°C, washed, and incubated with HRP-linked secondary antibody for 2 h. Chemiluminescence band detection was performed by Immobilon Forte Western HRP Substrate (Millipore). Fusion solo S (Vilber Lourmat, France) was used for protein band visualization. Image J was used for the quantification of the protein bands. The following antibodies were used: mouse anti-ZNT1 (Nishito et al., 2016), β-Actin (D6A8), Rabbit mAb HRP Conjugate (Cell signaling), HRP conjugated Goat-anti-mouse IgG (Jackson ImmonoResearch).

Knockdown of *SLC30A1* using siRNA

Cells were seeded at 2000 cell/well into a 96-well-plate with undiff-AKM (INS) medium. After 24 h, cells were transfected with ON-TARGETplus Human SLC30A1 siRNA or ON-TARGETplus Non-targeting Control siRNA (Horizon Discovery) in DharmaFECT 1 transfection reagent (Horizon Discovery), following the manufacturer's protocol. Cell transfection was carried out in Opti-MEM Reduced Serum medium diluted with AKM (INS) medium for 24 h. Transfected cells were treated with Compl and (-) Met media for 5 h and were collected for RNA extraction or western blot assay.

EdU incorporation

Cells were incubated with EdU/medium for 30 min after being cultured in various Zn conditions. Then the cells were fixed, permeabilized, and ready for EdU detection. The cells were incubated with a reaction cocktail (100 mM Tris-HCl pH 8.0, 4 mM $CuSO_4$, 50 mM Ascorbic acid, 594 Alexa Fluor Azide – 1/1000 dilution) for 30 min in the dark. The cells were treated with DAPI for nuclear staining. EdU- and DAPI-positive cells were quantified using MetaXpress cellular image analysis software (Molecular Devices).

TUNEL analysis

The TUNEL assay was performed using the In Situ Cell Death Detection Kit, Fluorescein (cat. No. 11684795910, Roche Applied Science, Mannheim, Germany).

Alkaline phosphatase staining

For alkaline phosphatase staining, differentiated cells were fixed with 4% paraformaldehyde (Nacalai Tesque), washed once in PBS, and stained with NBT/BCIP solution (Nacalai Tesque).

Assessment of extracellular ATP content

Undifferentiated hiPSCs were replated at 5 $\times 10^4$ cells/well into a 4-well-plate and cultured for 2 days in undiff-AKM (IGF1) with Zn addition (0 and 3 μM) media. The medium was collected for ATP analysis, and cells were harvested from the same wells for the calculation of DNA content. The extracellular ATP concentrations were determined by cell-titer glo analysis (Promega), and genomic DNA was purified from cells using FavorPrep DNA extraction kit (FAVORGEN). Extracellular ATP levels were normalized by DNA amount and calculated as relative values with the Zn3 culture group as 1.

Sphere formation and methionine deprivation

Undifferentiated hiPSCs cultured on two-dimensional plates pre-coated with SynthemaxII (Corning) were dissociated and replated onto 6-well suspension culture plates at a density of 5x10^6cells /well (Greiner Bio One#657185) and cultured at 37°C for 24 h to form spheres on a rotating orbital shaker at 95 rpm. Then, (-) Met pretreatment was done by culturing the cells for 5 h in StemFit KA01 ((-) Met) medium or control complete media (StemFit KA01+100 μM methionine) (Ajinomoto, Tokyo), before initiation of differentiation.

Pancreatic differentiation protocol in Figure 1

Initially, we used the following protocol for differentiation (Figure 1). Initiation of differentiation was done after 5 h complete or methionine deprivation pretreatment. The media used for the 5-stage β cell differentiation protocol was reported previously (Shahjalal et al., 2014; Nakashima et al. 2015), with minor modifications. Details are as follows. Differentiation was performed with cells in spheres (Figures 1A–1G) or in monolayers (Figure 1H).

Medium 1 (M1): Initiation of differentiation was done by replacing the culture with Medium 1, consisting of DMEM with 4,500 mg/L glucose supplemented with 3 μM CHIR99021 (Stemgent or Wako), 100 ng/mL recombinant human Activin-A (Cell Guidance Systems), and 2% B27 insulin supplement (Life Technologies). On days 1 and 2, the media was replaced with M1 medium without CHIR99021.

Medium 2 (M2): On days 3 and 4, the media was replaced with Medium 2, containing RPMI (Life Technologies) supplemented with 0.25 μM SANT-1 (Sigma), 50 ng/mL recombinant human FGF10 (Pepro Tech, Inc.) and 2% B27 insulin supplement.

Medium 3 (M3): From day 5, the media were replaced with Medium 3, containing DMEM with 4,500 mg/L glucose supplemented with 0.25 μM SANT-1, 0.1 μM LDN193189 (Sigma), 2 μM retinoic acid (RA; Stemgent), and 1% B27 insulin supplement.

Medium 4 (M4): From day 11 on, the media was changed to Medium 4, consisting of DMEM with 4,500 mg/L glucose supplemented with 0.1 μM LDN193189, 5 μM TGF-β type I receptor kinase inhibitor II (ALK5i) (Wako), 0.3 μM (-)-Indolactam V (ILV) (R&D Systems), and 1% B27 insulin supplement.

Medium 5 (M5): From day 13 to 25, cells were cultured in Medium 5, containing Knockout DMEM/F-12 (Life Technologies) supplemented with 50 ng/mL exendin-4 (Ex-4) (Cell Sciences, Inc.), 10 mM nicotinamide (NA) (Sigma), 1mM N-acetyl-L-cysteine (NAC) (Nacalai Tesque), 10 μM $ZnSO_4$ (Sigma), and 1% B27 insulin supplement. From day 5, media were replaced every 2 days with fresh media and growth factors.

All media were supplemented with L-Glutamine, PS, MEM Non-essential amino acid (NEAA; Life Technology), and 2-Mercaptoethanol (2-ME; Sigma).

Pretreatment of hiPSCs with AKM (Zn 0 / IGF)

hiPSCs were replated at 5 x 10^5 cells/well into 6-well-plate and cultured for 3 days with AKM (Zn0) supplemented with 100 ng/mL IGF1, then cells were harvested for real-time PCR analysis.

Mesoderm and ectoderm differentiation using AKM media

hiPSCs were replated at 3 x 10^4 cells/well into 96-well-plate and cultured for 3 days with AKM (Zn0) supplemented with 100 ng/mL IGF1, then used for differentiation. Mesoderm differentiation was induced by culturing hiPSCs in AKM (Zn0) supplemented with 100 ng/mL IGF1, 8 μM CHIR99021 and 25 ng/mL BMP4 (Takebe et al., 2017). Ectoderm differentiation was induced by culturing hiPSCs in AKM (Zn0) supplemented with 100 ng/mL IGF1, 250 nM LDN193189, 10 μM SB431542, and 5 μM XAV939 (Qi et al., 2017).

Endoderm differentiation using AKM media

(Figure 4) Initiation of differentiation was performed by replacing AK03N with or without KA01 ((-) Met) pretreatment, which was changed to M1-AKM (IGF1) supplemented with Zn at different concentrations or M1-AKM (INS). M1-AKM (IGF1): medium with AKM (Zn 0), supplemented with 0, 0.5, or 3 μM $ZnSO_4$, 3 μM CHIR99021, 100 ng/mL Activin-A, 100 ng/mL IGF1. M1-AKM (INS): StemFit Basic03 supplemented with 3 μM CHIR99021, 100 ng/mL Activin-A. On days 1 and 2, the media was replaced with a medium without CHIR99021.

Pancreatic differentiation using AKM medium

(Figures 4 and 5) After 5 h methionine deprivation pretreatment, initiation of differentiation was done by replacing maintenance media with M1-AKM. On day 3, the medium was replaced with medium S2. On day 5 (Figure 4) or day 6 (Figure 5), replaced with S3 media, and cells were cultured for 2 days. On day 7 (Figure 4) or day 8 (Figure 5), switched to S4 media and cultured for 5 days (Figure 5) or 6 days (Figure 4). On day 13, switched to S5 media. On day 21, then switched to S6 media.

Medium 1 (M1-AKM): Differentiation was initiated by replacing the medium with AKM (Zn 0), supplemented with 0, 0.5, or 3 μM $ZnSO_4$, 3 μM CHIR99021, 100 ng/mL recombinant human Activin-A, 100 ng/mL recombinant human IGF1 and 10 μM Y27632 (only 1 day). On days 1 and 2, the media was replaced with medium 1 without CHIR99021.

Stage 2 (S2-AKM): On days 3 and 4, the media was replaced with medium S2, containing StemFit AKM (Zn 0 or 0.5) supplemented with 0 or 0.5 μM $ZnSO_4$, 50 ng/mL KGF (Fujifilm-Wako) and 44 μg/mL Vitamin C (Sigma).

Stage 2-2 (S2-2): On day 5, the media was replaced with medium S2-2, containing StemFit Basic03 (Ajinomoto) (Zn 3), supplemented with 50 ng/mL KGF, 44 μg/mL Vitamin C (only Figure 5).

Stage 3 (S3): From day 5 or 6, the media were replaced with Medium S3, containing StemFit Basic03 (Ajinomoto), 50 ng/mL KGF, 0.25 μM SANT-1, 500 nM PdBU, 0.2 μM LDN193189, 2 μM RA, 44 μg/mL Vitamin C, and 10 μM Y27632. From day 7, the culture was switched to medium without LDN193189.

Stage 4 (S4): From day 7 or 8 to 12, the media were replaced with medium S4, containing StemFit Basic03 (Ajinomoto), supplemented with 50 ng/mL KGF, 0.25 μM SANT-1, 100 nM RA, 44 μg/mL Vitamin C, 5 ng/mL activin A and 10 μM Y27632.

Stage 5 (S5): From day 13 to 16, cells were cultured in medium S5, containing StemFit Basic03, supplemented with 10 μM Alk5i, 1 μM γ-Secretase Inhibitor XXI (GSXXI) (Sigma) 20 ng/mL Betacellulin (Pepro Tech, Inc.), 100 nM RA, 44 μg/mL Vitamin C, 1 μM L-3,3′,5-Triiodothyronine (T3) (Sigma), with or without 0.2 μM LDN193189, 0.25 μM SANT-1 and 10 μg/mL heparin (Sigma). From days 17-20, cells were cultured in the same medium without Vitamin C, LDN193189, and SANT-1. Also, RA concentration was changed from 100 nM to 25 nM.

Stage 6 (S6): From day 21, for cohort 1, cells were cultured in medium S6, containing StemFit Basic03, supplemented with 10 μM $ZnSO_4$. For cohorts 2 and 3, reaggregation of hiPSβ cells (Protocol referred below) was performed and cells were cultured in medium S6, containing MCDB 131 supplemented with 0.44 g/L glucose, 2% FAF-BSA, 10 μg/mL heparin, 1 μM $ZnSO_4$, 0.1% Trace Elements A (Corning) and 0.1% Trace Elements B (Corning). The cells were replenished with fresh media every other day.

Pancreatic differentiation using MCDB medium

Undifferentiated Ffl01s01 cells were cultured and differentiated following the published protocol (Velazco-Cruz et al., 2019) with some modifications. Briefly, undifferentiated hiPSCs cultured on two-dimensional plates pre-coated with SynthemaxII (Corning) were dissociated and replated onto 6-well suspension culture plates at a density of 5x10^6cells /well (Greiner Bio One#657185)

and cultured at 37°C for 48 h to form spheres on a rotating orbital shaker at 95 rpm. Differentiation was initiated by replacing the media with a Stage 1 (DE) media. On day 3, the medium was replaced with Stage 2 (PGT) media. On day 6, the medium was replaced with Stage 3 (PP1) media, and the cells were cultured for 2 days. On day 8, the medium was switched to Stage 4 (PP2) media and cultured for 5 days. On day 13, switched to Stage 5 (EN) media. On day 21, reaggregation of cell spheres was performed, and the medium was switched to Stage 6 (SC-β) media. Cell spheres were washed in PBS and incubated in TrypLE Select Enzyme (Thermo Fisher Scientific #12563029) for 10 min at 37°C. Spheres were mechanically dissociated using a P1000 pipette. Cells were then quenched with Stage 6 (SC-β) media and spun down, washed with Stage 6 (SC-β) media + Y27632 (10 μM), resuspended at approximately 1 x 10^6 cells in Stage 6 (SC-β) media + Y27632, then passed through a 100-μm CellStrainer (pluriSelect) to remove any residual undissociated clusters. The dissociated single cells were counted and seeded into a 6-well suspension culture plate (Greiner Bio One #657185) at a density of 3∼6 x 10^6 cells per well in Stage 6 (SC-β) medium + Y27632 and cultured in an incubator at 37°C with 95∼100 r.p.m. agitation. Medium changes were done every 48 h with Stage 6 (SC-β) medium and cultured up to day 35.

Stage 1 (DE): Differentiation was initiated by replacing the medium with MCDB 131 (Gibco) supplemented with 0.44 g/L glucose (Otsuka Pharmaceutical Factory, Inc.), 0.5% FAF-BSA (Proliant biologicals), 0.002% ITS-X (Gibco), 3 μM CHIR99021, 100 ng/mL recombinant human Activin-A and 10 μM Y27632. On days 1 and 2, the medium was replaced with Stage 1 (DE) media without CHIR99021 and Y27632.

Stage 2 (PGT): On days 3 and 4, the media was replaced with MCDB 131 supplemented with 0.44 g/L glucose, 0.5% FAF-BSA, 0.002% ITS-X, 50 ng/mL KGF (Fujifilm-Wako) and 44 μg/mL Vitamin C (Sigma).

Stage 3 (PP1): On day 6, the media was replaced with MCDB 131 supplemented with 0.44 g/L glucose, 0.5% FAF-BSA, 0.5% ITS-X, 50 ng/mL KGF, 0.25 μM SANT-1, 500 nM PdBU, 0.2 μM LDN193189, 2 μM RA, 44 μg/mL Vitamin C, and 10 μM Y27632.

Stage 4 (PP2): From day 8 to 12, the media were replaced with MCDB 131 supplemented with 0.44 g/L glucose, 0.5% FAF-BSA, 0.5% ITS-X, 50 ng/mL KGF, 0.25 μM SANT-1, 100 nM RA, 44 μg/mL Vitamin C, 5 ng/mL activin A and 10 μM Y27632. The cells were replenished with fresh media on day 10 and 12.

Stage 5 (EN): From day 13 to 16, cells were cultured in MCDB 131 supplemented with 3.6 g/L glucose, 0.5% FAF-BSA, 0.5% ITS-X, 10 μM Alk5i, 1 μM γ-Secretase Inhibitor XXI (GSXXI) (Sigma), 20 ng/mL Betacellulin (Pepro Tech, Inc.), 100 nM RA, 44 μg/mL Vitamin C, 1 μM L-3,3′,5-Triiodothyronine (T3) (Sigma), 0.25 μM SANT-1 and 10 μg/mL heparin (Sigma). From days 17–20, cells were cultured in the same medium without SANT-1 and RA concentration changed from 100 nM to 25 nM. The cells were replenished with fresh media on day 19.

Stage 6 (SC-β): From day 21, cells were cultured in MCDB 131 supplemented with 0.44 g/L glucose, 2% FAF-BSA, 10 μg/mL heparin, 1 μM $ZnSO_4$, 0.1% Trace Elements A (Corning) and 0.1% Trace Elements B (Corning). The cells were replenished with fresh media every other days.

Immunocytochemistry

For analysis of differentiated hiPSC spheres, cells were dissociated, replated on a 96-well plate, overnight cultured at 37°C, then subjected to immunostaining. Cells were fixed in 4% paraformaldehyde in PBS, permeabilized with 1% Triton X-100 (Nacalai Tesque), and were then blocked with 20% Blocking One (Nacalai Tesque, Japan) in PBST (0.1% Tween-20 in PBS). Antibodies were diluted in 20% Blocking One (Nacalai Tesque, Japan) in PBST (0.1% Tween-20 in PBS). Cells were counterstained with 6-diamidino-2-phenylindole (DAPI) (Roche Diagnostics, Switzerland). The following primary antibodies were used: mouse anti-OCT3/4 (Santa Cruz Biotechnology, sc-5279), goat anti-SOX17 (R&D Systems, AF1924), rabbit anti-SOX9 (Merck, AB5535), goat anti-PDX1 (R&D Systems, AF2419), guinea pig anti-INSULIN (Agilent Dako, IR002), rabbit anti-C-peptide (Cell Signaling), mouse anti-NKX6.1 (Developmental Studies Hybridoma Bank, F55A10), rabbit anti-SOMATOSTATIN (Sigma-Aldrich, SAB4502861), mouse anti-GLUCAGON (monoclonal, clone K79bB10; Sigma-Aldrich). Secondary antibodies conjugated to Alexa Fluor488, 647, or CF488, 568 were used to visualize primary antibodies. Positive cells versus total cells (DAPI-positive cells) were quantified using ImageXpress Micro cellular imaging system (Molecular Devices).

Real-time PCR analysis

RNA was extracted from iPS cells using the RNeasy micro-kit, or All prep (DNA/RNA) Micro Kit (Qiagen, Germany) or Cica geneusR RNA Prep Kit (For Tissue), and treated with DNase (Qiagen). One μg RNA was reverse-transcribed using PrimeScript™ RT Master Mix (Takara, Japan). The mRNA expression was quantified with SyberGreen on a StepOne Plus (Applied Biosystems, Foster City, CA). The PCR conditions were as follows: initial denaturation at 95°C for 30 s, then denaturation at 95°C for 5 s, annealing and extension at 60°C for 30sec, for up to 40 cycles. Target mRNA levels were expressed as arbitrary units and were determined using the ΔΔ CT method.

For Figure 3, PrimerArray Embryonic Stem Cells (Human) (TaKaRa #PH016) containing primer pairs optimized for real-time RT-PCR analysis of 88 genes associated with pluripotency and self-renewal of embryonic stem cells and 8 housekeeping genes were used. Primer sequences used for detecting *SLC30A* and *SLC39A* gene expression (Figures 2, S1, and S2), endoderm and pancreatic differentiation markers (Figures 3, 5, and S3–S6) and internal control markers are listed in Table S7.

Affymetrix microarray analysis and accession numbers

Undifferentiated cells, Toe hiPSC-derived day3 DE cells, day 5 PG cells, day 11 PP cells, day 13 EP cells, and day 25 EC cells were used to compare their gene expression profiles using GeneChip™ Human Gene 2.0 ST Array (Applied Biosystems). Microarray data are deposited under Gene Expression Omnibus (GEO) accession number GSE151794. Expression profiles of undifferentiated hiPSC/ESC cultured under (-) Met or control complete medium were compared with 201B7 hiPSCs (GEO accession number GSE151795) using Human Transcriptome Array (HTA) 2.0 (Applied Biosystems). Data from human KhES3 (GEO accession number GSE55285) (Shiraki et al., 2014) were used for comparison. Toe and 201B7cells were cultured with control complete StemFit AK medium or Met-deprived StemFit media for 5h. (KA01).

RNA sequencing

Ff-I01s01 undifferentiated hiPSCs were dissociated and plated at 5×10^5 cells/well on SynthemaxII-coated 6-well plates (Corning) and cultured at 37°C for 24 h, then cultured for 48 h with undiff-AKM (IGF1) medium with Zn addition (0, 0.5, 3, and 10 μM), then dissociated and harvested. RNA was extracted using the RNeasy micro-kit (Qiagen, Germany), and DNase I (Qiagen) treatment was performed according to the manufacturer's instructions.

A total amount of 1 μg RNA per sample was used for library preparation and RNA sequencing, performed by Novagene Co. Ltd. Briefly, sequencing libraries were generated using NEBNext® UltraTM RNA Library Prep Kit for Illumina® (NEB, USA), following the manufacturer's instructions. Index codes were added to attribute sequences to each sample. The clustering of the index-coded samples was performed on a cBot Cluster Generation System, using PE Cluster Kit cBot-HS (Illumina), following the manufacturer's instructions. After cluster generation, the library preparations were sequenced on an Illumina platform (Novaseq 6000PE150), and paired-end reads were generated. RNA-seq reads were processed with Subio Platform v1.24.5659. The pipeline is composed of fastp v0.20.0, HISAT2 v2.1.0, and StringTie v2.0.6 software and calculated with the GRCh38 genome and Ensembl's gene model of the same genome version. It outputs TPM and reverse-calculated count values, which we analyzed with the Subio Platform software afterward. The RNA-seq data are available in GEO-NCBI (accession number GSE152017).

Principal component analysis

We performed principal component analysis (PCA) to visualize the results and map the expression profile among undifferentiated cells, iPSC-derived differentiated cells on day 3 DE cells, day 5 PG cells, day 11 PP cells, day 13 EP cells and day 25 EC cells (Figure 1C). PCA was performed using JMP software (SAS Institute Inc., Cary, NC, USA).

Reaggregation of hiPSβ

We performed reaggregation of hiPSβ as previously described (Veres et al., 2019) with some modifications. Briefly, hiPSβ spheres were dissociated into single cells at the end of stage-5 differentiation. hiPSβ sphere (approximately 5×10^6 cells) were washed in PBS and incubated in TrypLE Select Enzyme (Thermo Fisher Scientific #12563029) for 20–30 min at 37°C. Spheres were mechanically dissociated using a P1000 pipette every 10 min. Cells were then quenched with DMEM +10% FBS and spun down, washed with stage-6 medium + Y27632 (10 μM), resuspended at approximately 1×10^6 cells in stage-6 medium + Y27632, then passed through a 100-μm CellStrainer (pluriSelect) to remove any residual undissociated clusters. The dissociated single cells were counted and seeded into a 6-well suspension culture plate (Greiner Bio One #657185) at a density of $3\sim6 \times 10^6$ cells per well in stage-6 medium + Y27632 and cultured in an incubator at 37°C with 95∼100 r.p.m. agitation. The endocrine cells self-aggregate into clusters within 24 h. Medium changes were done every 48 h with stage-6 medium and cultured up to day 38 or longer.

C-peptide release and content assay

C-peptide release and C-peptide content assay were performed as described previously (Sakano et al., 2014) with minor modifications. Briefly, differentiated cells were loaded on Transwell (Corning #3415) and pre-incubated for 4x 10 min + 30 min at 37°C in low glucose (2.5 mM ∼ 3.0 mM) HKRB buffer (HEPES Krebs-Ringer Bicarbonate buffer, Cosmo Bio) with 0.2% BSA, on an orbital shaker (70 rpm). The buffer was collected (Low glucose), and cells were further incubated in high glucose (20 mM) HKRB buffer with 0.2% BSA, at 37°C on an orbital shaker (70 rpm) for another 1 h. During 1 h incubation in high glucose buffer, 10% of supernatant was collected at 10 and 30 min and then added back to the same volumes of high glucose buffer. The collected culture supernatant was stored at -30°C until analysis. Cells were lysed, RNA and DNA were purified using AllPrep DNA/RNA Micro Kit (Qiagen). C-peptide secretion was measured using a human C-peptide ELISA Kit (Mercodia) and human C-peptide AlphaLISA kit (PerkinElmer). The amount of C-peptide was normalized to total DNA contents in the corresponding cell lysate. DNA contents corresponding to 1000 cells were used for normalization (Figure 5).

Dynamic GSIS

A perifusion system BRANDEL; SF-6 was used with a high-precision 6-channel dispenser pump in conjunction with 0.015" inlet and outlet two-stop tubing connected to 275-μL cell chamber. Stage 6 clusters and cadaveric human islets were washed with KRB twice and resuspended in 2 mM glucose KRB. Cells were then loaded onto the perifusion chamber. Cells were perfused with 2 mM glucose 90 min for equilibration. Then started with 2 mM glucose/KRB, 32 min, followed by 20 mM glucose / KRB for 28 min; 2 mM glucose / KRB, 32 min; then 30 mM KCL in 2 mM glucose / KRB for 16 min. The effluent was collected at a 100 μL/min flow rate with 2–8 min

collection points. Then clusters were harvested and lysed in RLT-plus solution, and DNA was purified by Allprep DNA/RNA micro kit (QIAGEN; 80284) and Qubit dsDNA High Sensitivity Assay Kit (ThermoFisher; Q32851). C-peptide secretion was quantified using the Human C-peptide AlphaLISA kit and normalized to total DNA contents or cell clusters (1000 cells).

Metabolite analysis

Undifferentiated hiPSCs were replated at 5 $\times 10^5$ cells/well into 6-well-plate and cultured for 2–3 days in undiff-AKM (IGF1) with Zn addition (0 and 3 μM) media. The media were collected, and cells were harvested for metabolite analysis. Metabolites measurements were performed using ultra-high-performance liquid chromatography equipped with tandem mass spectrometry, TQD (UPLC-MS/MS; Waters) based on a previous report (Jiang et al., 2009). Separation was achieved using a PALL 10K omega column. Briefly, cells were lysed using three cycles of freeze/thaw in 50% methanol. Samples were deproteinized using 33% acetonitrile and evaporated completely. Each sample was injected, and concentrations were calculated based on the standard curve obtained from serial dilution of standard solution for each metabolite. Intracellular metabolites ($[Metabolite]_i$) are obtained by normalizing the metabolites to total protein (μmol / g total protein). Extracellular metabolites ($[Metabolite]_E$) are obtained by subtracting the metabolites with reference (initially contained metabolites in the fresh medium) and normalized to 24 h, and the cell number (nmol / 24h /1x10^6 cells).

QUANTIFICATION AND STATISTICAL ANALYSIS

Individual data are shown or expressed as the mean ± standard deviation (SD). Each experiment was conducted with biological replicates ($\geq$ 3) and repeated multiple times. Differences between groups were analyzed by Student's *t*-tests; differences are shown as *$p < 0.05$, **$p < 0.01$, ***$p < 0.001$ or ****$p < 0.0001$; one-way ANOVA and Dunnett's multiple comparisons test; differences are shown as $^{\S}p < 0.05$, $^{\S\S}p < 0.01$, $^{\S\S\S}p < 0.001$, $^{\S\S\S\S}p < 0.0001$; respective statistical analysis and p-value are noted in each figure legend.